JOURNAL OF PETROLOGY | VOLUME 54 | NUMBER 3 | PAGES 539–574 | 2013 | doi:10.1093/petrology/egs077

Dendritic Crystallization: A Single Process for all the Textures of Olivine in Basalts?

BENOÎT WELSCH[1,2]*, FRANÇOIS FAURE[2], VINCENT FAMIN[1], ALAIN BARONNET[3] AND PATRICK BACHÈLERY[1,4]

[1]UNIVERSITÉ DE LA RÉUNION, LABORATOIRE GÉOSCIENCES, UMR-CNRS 7154 IPGP, 15 AVENUE RENÉ CASSIN, 97715 SAINT DENIS MESSAG CEDEX 9, LA RÉUNION, FRANCE

[2]UNIVERSITÉ DE LORRAINE, CNRS-CENTRE DE RECHERCHES PÉTROGRAPHIQUES ET GÉOCHIMIQUES, UPR 2300, 15 RUE NOTRE DAME DES PAUVRES, 54501 VANDOEUVRE-LÈS-NANCY, FRANCE

[3]UNIVERSITÉ AIX-MARSEILLE, CINAM-CNRS, UPR 3118, CAMPUS LUMINY, CASE 913, 13288 MARSEILLES CEDEX 9, FRANCE

[4]UNIVERSITÉ DE CLERMONT-FERRAND II, LABORATOIRE MAGMAS & VOLCANS, OPGC, UMR 6524, 24 AVENUE DES LANDAIS, 63177 AUBIÈRE, FRANCE

RECEIVED OCTOBER 21, 2011; ACCEPTED SEPTEMBER 21, 2012
ADVANCE ACCESS PUBLICATION NOVEMBER 19, 2012

The olivine macrocrysts found in oceanites, picrites and magnesian basalts erupted at hotspot volcanoes are generally interpreted either as phenocrysts crystallized from the magma or as xenocrysts extracted from a deforming cumulate. To constrain the origin of these crystals we studied their texture and composition at Piton de la Fournaise volcano, La Réunion. We show that macrocrysts are organized and subdivided into parallel units; this suggests a crystallization by dendritic growth and ripening rather than by a complex combination of paired nucleation, crystal aggregation or synneusis. Dendritic growth is also evidenced by the occurrence of hollow faces, P-rich zones, melt and Cr-spinel inclusions formed from the accumulation of slow diffusing impurities (P, Cr, Al) in the liquid at the contact with rapid-growing olivine. We suggest that early dendritic crystallization may even cause branch misorientations and lattice mismatches, yielding subgrain boundaries, dislocation lamellae and to a certain extent undulose extinction, which have all been formerly interpreted in terms of plastic intracrystalline deformation. We interpret olivine macrocrysts as phenocrysts crystallized under a strong degree of undercooling ($-\Delta T > 60^{\circ}C$), and derived from a harrisitic mush formed on the cold walls of the magma reservoir. Given the growth shapes indicated by P zoning patterns and external faces, the olivine macrocrysts (which consist of groups of several subcrystals) have grown in suspension within the liquid and were neither aggregated into a dense cumulate nor corroded, shocked or deformed before or during their transport to the surface. The major consequence of our study is that most olivine macrocrysts are not xenocrysts, and very few of them, if any, have experienced intracrystalline deformation. The importance of deforming (creeping) cumulate bodies, thought to accommodate the spreading of basaltic volcanoes in La Réunion and Hawaii, may hence have been overestimated.

KEY WORDS: *olivine; dendrite; magma chamber*

INTRODUCTION

Olivine is a major constituent of the Earth's upper mantle and also a crystallization product of magnesium-rich magmas on their way to the surface. As a consequence, it is of prime importance to be able to use olivine as a geochemical and/or petrological tracer of physico-chemical processes occurring during the genesis or ascent of magmas. Unfortunately, assessing the origin of olivine crystals transported in magmas remains problematic because chemical re-equilibration (owing to fast Fe–Mg lattice interdiffusion, Buening & Buseck, 1973; Chakraborty, 1997; Dohmen *et al.*, 2007) erases part of the geochemical information related to their early stage of

*Corresponding author. E-mail: benoit.welsch@univ-reunion.fr or bwelsch@hawaii.edu
Present address: University of Hawaii at Manoa, SOEST, 1680 East-West Road, Honolulu, HI 96822, USA.

© The Author 2012. Published by Oxford University Press. All rights reserved. For Permissions, please e-mail: journals.permissions@oup.com

Downloaded from http://petrology.oxfordjournals.org/ at University of Hawaii at Manoa Library on February 13, 2013

crystallization. This has led researchers to focus on the texture of olivine, which is very sensitive to the thermodynamic and kinetic conditions of crystallization and hence may be used to reconstruct the history of crystals and their host magma.

Helz (1987) made the largest inventory of textures within the olivine-rich basalts erupted in 1959 at Kilauea Iki (Hawaii). She reported up to seven olivine classes, including [i] irregular blocky crystals with dislocation lamellae, [ii] euhedral or skeletal crystals, [iii] rounded crystals, [iv] angular or conchoidal fragments, [v] euhedral crystals containing sulphide inclusions, [vi] dunitic aggregates and [vii] megacrysts (see Supplementary Data, Appendix 1, available for downloading at http://www.petrology.oxfordjournals.org). Similar olivine textures have been described in lavas from La Réunion (Albarède & Tamagnan, 1988), Cyprus (Boudier, 1991), North Siberia (Arndt *et al.*, 1995), New Zealand (Ninomiya & Arai, 1998), West Greenland (Larsen & Pedersen, 2000), the Izu–Mariana arc (Amma-Miyasaka & Nakagawa, 2002), Japan Trench (Hirano *et al.*, 2004) and Solomon Islands (Rohrbach *et al.*, 2005). These textures fall into two categories: phenocrysts, resulting from crystallization only (types [ii], [v] and [vii]); xenocrysts (types [i], [iii], [iv] and [vi]), resulting from post-crystallization deformation or resorption processes.

However, despite the consistency of observations, there is no consensus about the nature of crystallization mechanisms and the causes of deformation or resorption of olivine. For instance, Helz (1987) interpreted phenocrysts as the products of fractional crystallization (in a reservoir) and xenocrysts as tectonized olivine cumulates. Drever & Johnston (1957) suggested that skeletal crystals [ii] are formed by rapid olivine growth during the emplacement of lavas. Natland (2003) proposed that phenocrysts can become 'xenocrysts' by colliding during their transport to the surface, resulting in crystal deformation (type [i]), corrosion (type [iii]) or fragmentation (type [iv]). At the other extreme, it has been argued by Schwindinger & Anderson (1989) and Schwindinger (1999) that phenocrysts as well as xenocrysts result from a single process called synneusis (Vogt, 1921; Vance, 1969); that is, an oriented attachment of crystals swimming together in the magma (Supplementary Data, Appendix 2). More recently, Milman-Barris *et al.* (2008) discovered P-, Cr- and Al-rich zones in terrestrial and Martian olivines, outlining processes of impurity uptake enhanced by the rapid growth of the mineral.

To improve our understanding of olivine textures and their interpretation, we studied olivine crystals from Piton de la Fournaise, La Réunion. One advantage of studying the eruption products of this shield volcano is that they frequently contain large amounts of olivine crystals in lapilli, lavas and dunite enclaves, thereby allowing an observation of crystals in two and three dimensions. Another advantage is the extensive set of geophysical data recorded during the recent eruptions of olivine-rich basalts (January 2002, February 2005, December 2005 and April 2007), which can be compared with the results of our petrological approach. Because the origin of olivine at Piton de la Fournaise is still debated (Albarède & Tamagnan, 1988; Famin *et al.*, 2009), we re-examined the criteria discriminating xenocrysts from phenocrysts, and the applicability of processes such as crystal aggregation, synneusis, heterogeneous nucleation and parallel growth. Our petrological study indicates that none of these processes is consistent with the observations. We show rather that the whole suite of olivine textures and compositions observed can be explained by a single process of dendritic crystallization and ripening within the melt (a dendrite being a branching crystal made of several units, in contrast to euhedral or skeletal crystals, which are made of only one unit). These results not only provide an integrated explanation for the formation of olivine textures at Piton de la Fournaise; they also have critical implications for the dynamic processes occurring in other basaltic systems such as Hawaii.

GEOLOGICAL SETTING

The emerged part of La Réunion island includes a now inactive volcano, the Piton des Neiges (2·1–0·012 Ma, McDougall, 1971; Deniel *et al.*, 1992), and an active volcano, the Piton de la Fournaise (0·45 Ma up to present; Albarède *et al.*, 1997; Merle *et al.*, 2010; for a review see Lénat *et al.*, 2012). Both edifices are made of aphyric basalts and porphyritic olivine-rich basalts. The aphyric basalts were called 'Steady State Basalts' by Albarède *et al.* (1997) because of their uniform bulk MgO contents of 6–8 wt % MgO. In contrast, the olivine-rich basalts have a larger chemical spectrum with magnesian basalts at 9–12 wt % MgO, picrites at >12 wt % MgO (Le Bas, 2000) and oceanites at >20 wt % MgO (using the terminology of Lacroix, 1923). Studies of the recent eruptive products from Piton de la Fournaise have shown that the matrix glasses of the aphyric and olivine-rich basalts have a composition similar to the bulk composition of the Steady State Basalts (Albarède *et al.*, 1997; Boivin & Bachèlery, 2009; Famin *et al.*, 2009; Welsch et *al.*, 2009; Salaün *et al.*, 2010). Albarède & Tamagnan (1988) have also proposed that the olivine-rich basalts contain both phenocrysts and xenocrysts.

Two models have been proposed for the coexistence of olivine-rich and aphyric basalts at Piton de la Fournaise. In the first model, a parental magma (9–16 wt % MgO) differentiates into basalt by crystallization and settling of olivine phenocrysts at the bottom of a magma chamber (Lacroix, 1936; Kieffer *et al.*, 1977; Ludden, 1978; Clocchiatti *et al.*, 1979; Fisk *et al.*, 1988; Famin et al., 2009; Villemant

Downloaded from http://petrology.oxfordjournals.org/ at University of Hawaii at Manoa Library on February 13, 2013

et al., 2009). Aphyric basalts result from the removal of olivine, and olivine-rich basalts from the cumulative counterpart. In the second model, the parental magmas are differentiated (≤7 wt % MgO) and percolate through conduits filled with olivine-rich crystal mushes (Albarède *et al.*, 1997; Bureau *et al.*, 1998*a*, 1999; Vlastélic *et al.*, 2005, 2007). The rising magmas interact with genetically unrelated olivine, yielding homogenized liquids at the surface with occasional olivine xenocrysts extracted from the mushy conduits by stronger magma pulses. It is worthwhile noting that the low forsterite content of olivine macrocrysts ($Fo_{87–83}$) and the low volatile concentration in their melt inclusions (<1 wt % H_2O and <0·1 wt% CO_2) are clear indicators that these crystals come from the crust, and not from the mantle (depth <3·5 km; P<100 MPa; Bureau *et al.*, 1998*a*, 1998*b*; Famin *et al.*, 2009).

Based on ground deformation studies and the location of seismic swarms, three magma storage zones have been proposed for Piton de la Fournaise: (1) a deep reservoir located beneath the oceanic crust at 15 km depth; (2) an intermediate reservoir at the base of the volcanic edifice at 7 km depth; (3) a shallow reservoir at ~2·5 km depth; that is, near sea level (Aki & Ferrazzini, 2000; Peltier *et al.*, 2009; Lénat *et al.*, 2012). The shallowest reservoir has been shown to be active during the olivine-rich basalt eruptions of January 2002, February 2005, December 2005 and April 2007 (Peltier *et al.*, 2009). Up to five refilling events have been evidenced for the period 1998–2007, but none of them occurred during the eruptions of December 2005 and April 2007 (see Coppola *et al.*, 2009, and references therein).

SAMPLING AND ANALYTICAL TECHNIQUES

Eleven olivine-rich lava samples were collected and quenched in water during the eruptions of January 2002, February 2005, December 2005 and April 2007 (Fig. 1). In addition, nine olivine-rich basalt samples were also collected after the natural solidification of lava flows. Dunites were found as enclaves (diameter ø 10–100 mm) in the solidified flows of the April 2007 eruption, and as ejecta at Piton Chisny (a basaltic cone of age ~1 ka; Upton *et al.*, 2000) and Piton Caille (an oceanite cone of age ~5 ka; Bureau *et al.*, 1998*b*). At this last location, olivine-rich lapilli were also sampled.

Major element analyses of bulk lava samples were performed with a Panalytical AXIOS X-ray fluorescence spectrometer at the University of La Réunion. The spectrometer was calibrated using eight international basic rock standards (NCS standards DC71301, DC72301, DC72302, DC71304, DC73303; CRPG-CNRS standard BE-N; USGS standards BCR-2 and BIR-1). The calibration was then checked again with the BHVO-2 USGS basalt standard, yielding an uncertainty on concentration measurements of 0·5–1% for major oxides and 1–5% for minor oxides.

The lava samples were also mounted in epoxy and prepared as polished thin sections for optical microscopic examination. The orientation and indexation of olivine crystal faces were determined by measuring the angles between the observed faces, taking into account lens distortion at the periphery of the images. The mesostasis-free olivine crystals from Piton Caille were imaged with secondary electrons using the JEOL JSM-6320 F scanning electron microscope (SEM) at CINaM-CNRS of the University of Aix-Marseille (France), equipped with a cold field-emission source and tuned at 3 keV. These crystals were previously glued onto a sticky graphite tape and coated with an evaporated 20 nm thick amorphous C layer for electron conduction. Some other crystals from Piton Caille were also photographed using a stereomicroscope in the three directions, using the bracketing technique (i.e. high dynamic range photography) and the Bracketeer 3.0 software (http://pangeasoft.net/pano/bracketeer/). For textural comparisons, the habit (i.e. the 3D shape of the crystal polyhedron), forms (i.e. the sets of symmetry-equivalent faces), interfacial angles, cleavages and twinning laws of forsteritic olivine were computed and drawn with the SHAPE 7.2 software (Dowty, 1980*a*, 1987; Fig. 2).

Major element compositions of the various phases were determined using a CAMECA SX-100 electron probe micro-analyser (EPMA) at the University of Nancy (France), tuned at 15 kV voltage, 10 nA current and 10 s peak counting time (Na measured first). Natural and synthetic mineral standards were used for calibration: orthoclase (Si, K), albite (Na, Al), wollastonite (Ca), hematite (Fe), olivine (Mg), pyrophanite (Ti, Mn), NiO (Ni), $KTi_2(PO_4)_3$ (P), Cr_2O_3 (Cr). Minerals were analysed with the beam focused at 1–2 μm. Matrix glasses were analysed with the beam defocused to 20 μm to reduce alkali loss. Melt inclusions were not re-homogenized before analysis, and no correction for possible post-entrapment chemical changes (epitaxial crystallization or iron loss by diffusion) was applied. Analytical uncertainty (1σ) is 1–2% for major elements, 5–15% for minor elements and 50–100% for trace elements. Detection limit is in the range 0·05–0·15 wt % for CaO, K_2O, TiO_2, P_2O_5 and Cr_2O_3, and 0·15–0·2 wt % for SiO_2, Al_2O_3, FeOt, MnO, MgO, Na_2O and NiO. Chemical mapping of P in olivine was made with the CAMECA SX-100 EPMA of Université Pierre & Marie Curie, Paris VI (France). Mapping was carried out on sections of olivine crystals with analytical conditions similar to those used by Milman-Barris *et al.* (2008). Depending on the size of the analyzed area, the beam was tuned at 15–30 kV, 300–500 nA with ~1 μm step and 200–400 ms dwell time. The scanning mode of the beam was controlled by plate

Downloaded from http://petrology.oxfordjournals.org/ at University of Hawaii at Manoa Library on February 13, 2013

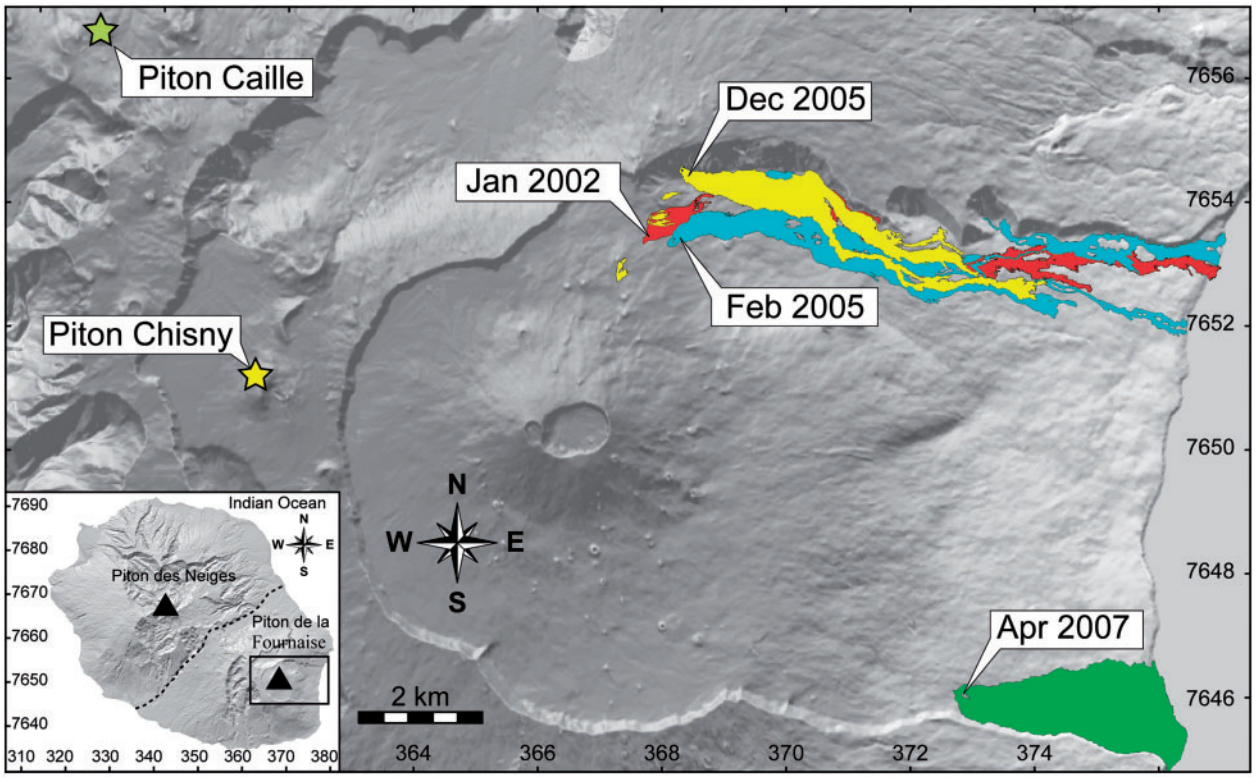

Fig. 1. Sampling sites at Piton de la Fournaise volcano (La Réunion Island, units in km UTM 40). Modified from Servadio *et al.* (2008).

displacement. The intensity of P, Cr, Al and Ca was determined with LTAP, LLIF, TAP and LPET crystals, respectively. The X-ray maps were each collected after 28–58 h running.

OLIVINE COMPOSITIONS AND TEXTURES

The compositions of the bulk-rock samples are given in Table 1. Their textures are shown in Fig. 3. The lava samples contain various amounts of crystals and vesicles in a glassy matrix (Fig. 3a–h). Crystals comprise macrocrysts (ø 0·5–10 mm), mesocrysts (ø 0·1–0·5 mm) and microcrysts (ø < 0·1 mm). The terms macrocryst, mesocryst and microcryst are hereafter used rather than phenocryst, microphenocryst and microlite because they are strictly descriptive and devoid of petrogenetic interpretation. Macrocrysts are exclusively olivine. Mesocrysts are either olivine or an assemblage of clinopyroxene + plagioclase. They have been studied previously (Welsch *et al.*, 2009), but olivine mesocrysts are re-investigated here as they are used for a comparison with the textures of the macrocrysts. Microcrysts are olivine, clinopyroxene, plagioclase and sometimes Fe–Ti-oxide. They were also investigated by Welsch *et al.* (2009) and will not be considered further in this study. Lapilli samples from Piton Caille consist of olivine macrocrysts (i.e. no mesocrysts observed) separated from their mesostasis by natural weathering, and only altered brown–red glass remains in the interstices or as a residual coating on the crystals.

The lava samples collected on the first days of the eruptions are mostly poor in olivine macrocrysts (Fig. 3a–f). They are Steady State Basalts at 7·32–7·50 wt % MgO, magnesian basalts at 9·04–11·31 wt % MgO, and picrites at 12·10–18·47 wt % MgO (Table 1). Steady State Basalts are aphyric, whereas magnesian basalts (Fig. 3c and d) and picrites (Fig. 3e and f) contain a few macrocrysts and/or abundant olivine mesocrysts, a reason why the hand specimens may appear aphyric like the Steady State Basalts (Fig. 3a). The oceanite samples collected during the later days of the eruptions have 20·98–29·19 wt % MgO (Table 1) because they contain more olivine macrocrysts (Fig. 3g and h). As a consequence, the bulk composition of the lava samples shows a systematic enrichment in MgO during the course of each eruption (January 2002, February 2005, December 2005 and April 2007, Table 1) owing to the increasing proportion of olivine macrocrysts (Vlastélic *et al.*, 2007; Peltier *et al.*, 2008). Dunite samples have compositions in the range 43·00–44·40 wt % MgO. They contain olivine macro- and/or mesocrysts in contact with each other or with minor amounts of interstitial glass and are devoid of vesicles (Fig. 3i and j).

Downloaded from http://petrology.oxfordjournals.org/ at University of Hawaii at Manoa Library on February 13, 2013

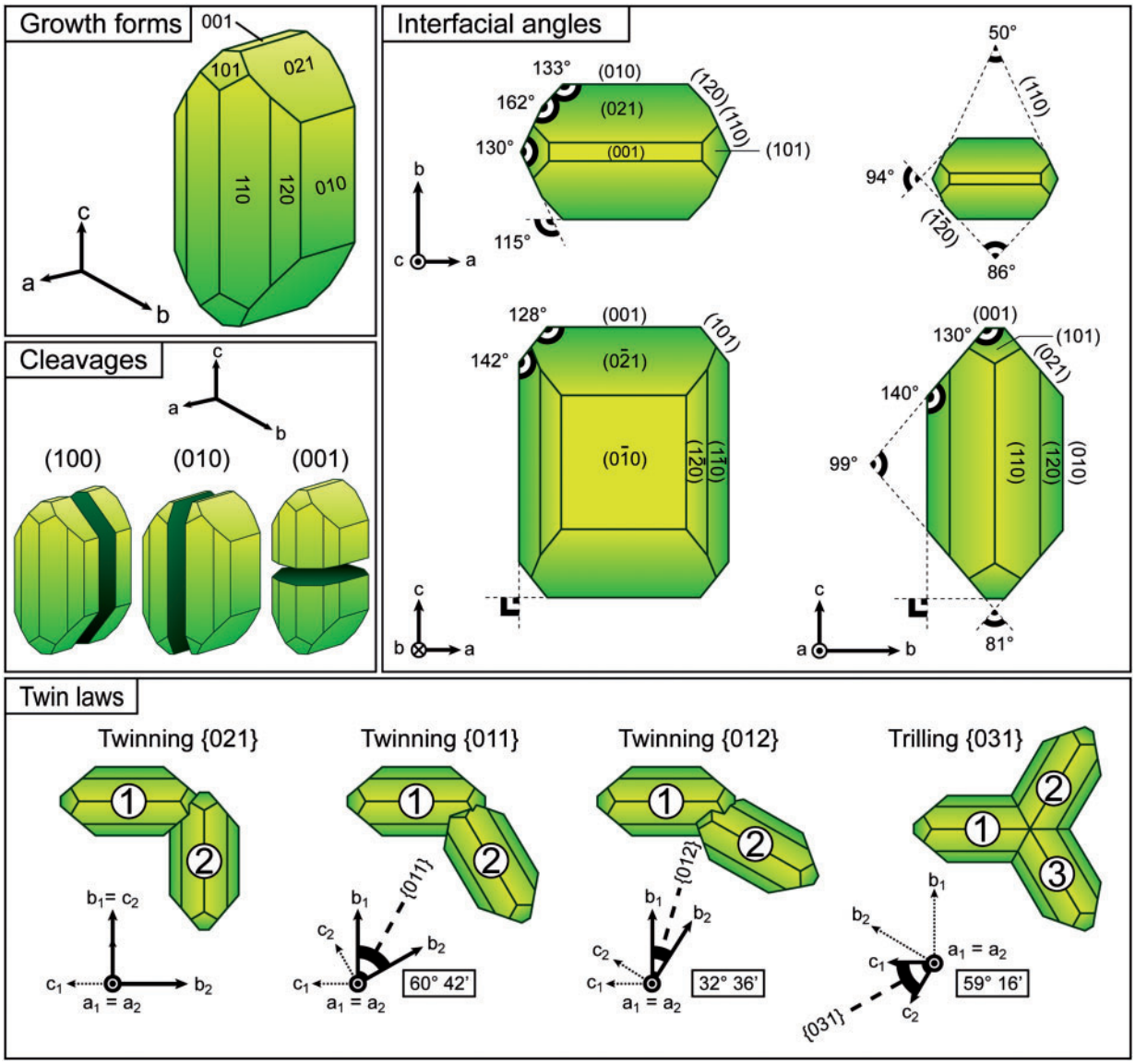

Fig. 2. Mineralogical data for forsteritic olivine. Crystal shape and interfacial angles were calculated using the software SHAPE 7.2 (Dowty, 1980*a*, 1987) for pure forsterite in the 2/*m* 2/*m* 2/*m* point group space with unit-cell parameters $a = 4{\cdot}756$, $b = 10{\cdot}195$, $c = 5{\cdot}981$ Å (Deer *et al.*, 1963). For a euhedral crystal with a shape ratio of $a{:}b{:}c = 1{\cdot}5{:}1{:}2$, the prominence of the different forms was controlled using reference central distances at {010} 0·46, {110} 0·64, {021} 0·64, {101} 0·98, {001} 0·92 and {120} 0·62. The interfacial angles are invariant whatever the shape ratio and the plane of section (law of constant angles; Steno, 1669; Romé de l'Isle, 1783). Distinct to perfect cleavages occur along the planes (010), (100) and (001). The angular relationships of the four twinning laws of olivine are shown after Dodd & Calef (1971). All olivine twins have a mutual *a*-axis whatever the twinning law. The angle between their respective *b*- or *c*-axes discriminates the twinning plane. Simple twinning is occasional in the planes {021}, {011} and {012}. It should be noted that the twinning {021} has been misindexed as {100} in the literature. Also represented is the trilling {031} proposed by Burri (1935).

Olivine and glass compositions

Representative compositions of olivine crystals and matrix glasses are given in Table 2. Matrix glasses of the 2002–2007 lavas have homogeneous compositions with 49–50 wt % SiO_2, 13·5–14·5 wt % Al_2O_3, 10–12 wt % FeOt, <0·3 wt % MnO, 5–7 wt % MgO, 10–12 wt % CaO, 2·3–2·9 wt % Na_2O, 0·6–0·9 wt % K_2O, <0·08 wt % Cr_2O_3, 2·8–3·3 wt % TiO_2, undetected NiO and 0·3–0·6 wt % P_2O_5, similar to the bulk contents of Steady State Basalts (Albarède *et al.*, 1997). The bulk and glass compositions of Piton Caille lapilli samples were not analysed because of the pronounced weathering of the interstitial glass between the olivine macrocrysts.

Olivine macrocrysts have a composition of $Fo_{87–85}$ in lapilli samples from Piton Caille (Bureau *et al.*, 1998*a*, 1998*b*). They are $Fo_{85–83}$ in the 2002–2007 lavas, whereas

Downloaded from http://petrology.oxfordjournals.org/ at University of Hawaii at Manoa Library on February 13, 2013

Table 1: Bulk chemical composition of lavas and dunite samples

	Jan 2002						Feb 2005				
	Day 2	Day 5	Day 9	Day 10	Day 12		Day 2	Day 6	Day 7	Day 9	Day 10
Sample:	020106-2	020109-2	020113-1	020114-1	020116-1		0502-181	0502-221	0502-231	0502-251	0502-261
Type:	Mg-Basalt	Picrite	Oceanite	Oceanite	Picrite		Picrite	Mg-Basalt	Mg-Basalt	Oceanite	Oceanite
SiO_2	47·88	46·92	43·15	44·23	46·29	SiO_2	47·41	48·14	48·2	44·88	45·03
Al_2O_3	13·09	11·9	6·66	7·98	10·04	Al_2O_3	11·7	12·86	12·74	8·43	8·66
Fe_2O_3	12·99	13·22	14·6	14·24	13·94	Fe_2O_3	13·82	13·14	13·12	14·26	14·06
MnO	0·17	0·17	0·18	0·18	0·18	MnO	0·19	0·18	0·18	0·19	0·19
MgO	10·36	13·7	28·13	24·49	18·47	MgO	14·29	11·02	11·31	22·86	22·07
CaO	10·43	9·43	5·32	6·33	7·9	CaO	9·35	10·23	10·22	6·76	6·97
Na_2O	2·41	2·18	1·18	1·42	1·8	Na_2O	2·24	2·44	2·43	1·6	1·64
K_2O	0·63	0·58	0·28	0·35	0·45	K_2O	0·58	0·63	0·63	0·4	0·42
TiO_2	2·42	2·19	1·23	1·48	1·86	TiO_2	2·14	2·35	2·33	1·55	1·6
P_2O_5	0·28	0·24	0·15	0·17	0·21	P_2O_5	0·28	0·3	0·29	0·21	0·21
LOI	−0·73	−0·59	−0·83	−0·82	−0·76	LOI	−1·53	−1·19	−0·99	−0·99	−0·75
Total	99·93	99·94	100·05	100·05	100·38	Total	100·46	100·12	100·45	100·13	100·1

	Dec 2005							
	Day 2	Day 5	Day 5	Day 18	Day 24	Feb 2007	Mar 2007	Chisny
Sample:	0512-271	0512-301	0512-303	0601-091	0601-181	070218-3	070331-1	—
Type:	Mg-Basalt	Mg-Basalt	Mg-Basalt	Oceanite	Oceanite	Basalt	Basalt	Dunite
SiO_2	47·06	48·28	48·34	43·7	43·53	48·86	48·89	38·92
Al_2O_3	12·21	13·44	13·34	7·64	7·07	13·88	13·82	0·64
Fe_2O_3	13·36	12·91	12·89	14·31	14·63	12·7	12·51	17·23
MnO	0·18	0·18	0·18	0·19	0·19	0·17	0·17	0·22
MgO	12·1	9·04	9·44	24·52	26·4	7·03	7·12	43·27
CaO	10·22	10·88	10·76	6·31	5·78	11·12	11·1	0·38
Na_2O	2·35	2·61	2·6	1·49	1·33	2·44	2·44	0·03
K_2O	0·61	0·65	0·64	0·34	0·3	0·64	0·64	0·01
TiO_2	2·36	2·62	2·59	1·48	1·37	2·64	2·64	0·14
P_2O_5	0·28	0·32	0·31	0·18	0·17	0·29	0·29	b.d.l.
LOI	−0·51	−0·85	−0·57	−0·62	−0·45	−1·09	−0·44	−1·22
Total	100·31	100·15	100·63	99·57	100·31	98·83	99·33	99·61

	Apr 2007											
	Day 1	Day 2	Day 3	Day 4	Day 5	Day 6	Day 7	Day 16	Day 19	Day 24	Day 27	Day 28
Sample:	070402-1	070403-1	70404	070405-1	70406	070407-1	070408-1	070417-1	070420-2	070425-1 F	070428-1	070429-1
Type:	Basalt	Basalt	Basalt	Oceanite	Oceanite	Oceanite	Oceanite	Oceanite	Oceanite	Oceanite	Oceanite	Oceanite
SiO_2	48·54	48·83	48·88	45·63	45·39	42·9	42·88	43·57	42·86	43·55	43·53	43·6
Al_2O_3	13·62	13·65	13·7	8·75	8·52	5·74	5·69	6·2	5·81	6·21	6·7	6·22
Fe_2O_3	12·507	12·738	12·714	14·148	14·067	14·925	15·009	14·97	14·856	14·976	14·69	15·018
MnO	0·17	0·17	0·17	0·18	0·18	0·19	0·19	0·19	0·19	0·19	0·19	0·19

(continued)

Downloaded from http://petrology.oxfordjournals.org/ at University of Hawaii at Manoa Library on February 13, 2013

Table 1: Continued

	Apr 2007											
	Day 1	Day 2	Day 3	Day 4	Day 5	Day 6	Day 7	Day 16	Day 19	Day 24	Day 27	Day 28
Sample:	070402-1	070403-1	70404	070405-1	70406	070407-1	070408-1	070417-1	070420-2	070425-1 F	070428-1	070429-1
Type:	Basalt	Basalt	Basalt	Oceanite	Oceanite	Oceanite	Oceanite	Oceanite	Oceanite	Oceanite	Oceanite	Oceanite
MgO	7·32	7·5	7·34	20·98	21·48	28·94	29·19	27·94	28·71	28·07	26·64	27·94
CaO	10·88	11·04	11·1	7·1	6·9	4·62	4·56	5·03	4·7	5·06	5·33	5·06
Na_2O	2·26	2·37	2·54	1·64	1·58	1·01	0·99	1·09	1·02	1·16	1·17	1·16
K_2O	0·62	0·67	0·7	0·42	0·39	0·25	0·25	0·27	0·26	0·31	0·3	0·33
TiO_2	2·61	2·61	2·62	1·67	1·63	1·09	1·07	1·17	1·09	1·16	1·24	1·16
P_2O_5	0·29	0·3	0·3	0·18	0·18	0·11	0·11	0·13	0·11	0·13	0·13	0·13
LOI	−0·65	−0·8	−0·68	−1·11	−0·95	−1·15	−1·25	−1·18	−1·23	−1·3	−1·15	−1·09
Total	98·32	99·21	99·52	99·9	99·7	99·06	99·14	99·8	98·79	99·95	99·18	100·14

Data for January 2002, February 2005 and December 2005 eruptions come from Vlastélic *et al.* (2007). Data for the dunite sample from Piton Chisny are from Upton *et al.* (2000). LOI, loss on ignition.

the olivine mesocrysts are in the range $Fo_{84–81}$. Olivine crystals from dunite enclaves of the April 2007 eruption and Piton Caille were not analysed; those from Piton Chisny are Fo_{82} (Upton *et al.*, 2000). The composition of olivine is homogeneous from one crystal to another within each population (macrocrysts, mesocrysts and dunites) in a given sample (variations in Fo $\leq$3%), and constant from core to edges (variations in Fo $\leq$1%), except in an $\sim$10 μm thick rim enriched in FeO ($Fo_{82–78}$). The calculated Fe–Mg partition coefficients (K_D of Roeder & Emslie, 1970; Toplis, 2005) indicate that the matrix glasses are in apparent equilibrium with the Fe-rich rims ($K_D = 0{\cdot}3 \pm 0{\cdot}03$) but not with cores ($K_D < 0{\cdot}27$, Table 2). Rims are also enriched in CaO (0·3–0·45 wt %), and depleted in NiO (<0·23 wt %) relative to the cores (0·20–0·37 wt % CaO; 0·24–0·46 wt % NiO). Olivine macro- and mesocrysts contain traces of Al_2O_3 (<0·1 wt %), MnO (<0·43 wt %), CaO (0·2–0·37 wt %), TiO_2 (<0·09 wt %), NiO (0·24–0·46 wt %) and Cr_2O_3 (<0·09 wt %).

Olivine textures

Macrocrysts in lavas and lapilli

The textures of olivine macrocrysts are listed in Table 3 and illustrated in Fig. 4. Olivine macrocrysts in the 2002–2007 lavas and Piton Caille lapilli are either single crystal units (Figs 5a, c, f and 6a–d, f) or, more frequently, groups of several crystal units (Figs 5b, d, e, 6e and 7–12) similar to the clusters described by Schwindinger & Anderson (1989).

Habit of crystal units. Each crystal unit has a polyhedral habit with well-developed growth forms {010}, {110}, {021} and {101}, and occasionally {001} and {120} (Figs 5, 7c–e and 8–12). Some crystal units display a skeletal habit: their faces {021}, {001} and, less frequently, {110} and {010} are re-entrant (Martin & MacLean, 1973; Donaldson, 1976; Figs 6a–e and 7a, b). In this case, their hollow faces have a large central funnel-shaped cavity with terraces (i.e. concentric benches parallel to external faces and separated by a gap, Fig. 7a) as described by Faure *et al.* (2003*a*). As shown in Fig. 7a, each terrace constitutes a new envelope of the growing crystal unit. In some crystals (Fig. 6b, c, e), the hollow faces may be also flat-bottomed with a melt inclusion underneath. Their trains of steps face inwards with sharp borders (Fig. 6a–e), evidencing a preferential growth at the edges and summits of the crystal.

Polyhedral and skeletal crystal units have sharper edges in lapilli (Figs 5–8) and in the glass-rich mesostasis of rapidly cooled zones of water-quenched lavas (Figs 9c–f, 10a–d, f), and more rounded shapes in the glass-poor mesostasis of air-cooled lavas and slowly cooled zones of water-quenched lavas (Figs 9a, b and 10e). In the latter case, groups of rounded crystal units are similar to the amoeboid texture of olivine type [iii] of Helz (1987) (Supplementary Data, Appendix 1). Most polyhedral and skeletal units have a habit slightly elongated along the *c*-axis, with a shape ratio close to that of standard olivine (e.g. $a:b:c = 1{:}1{\cdot}2{:}2{\cdot}2$ in Piton Caille unit 2 of Fig. 7e, and $1{\cdot}5{:}1{:}2$ in Fig. 2). However, some units show an extreme elongation along the *a*-axis (e.g. $a:b:c = 6{\cdot}6{:}1{:}1{\cdot}7$ in Fig. 7d; see also Figs 5c, d, 6d, e and 7c) similar to the spinifex-textured olivine of komatiites (Viljoen & Viljoen, 1969; Pyke *et al.*, 1973). It should be noted that elongated crystals can have one unfaceted extremity (Fig. 7c and d), suggesting that the crystal grew from a substrate.

All the units of a given group show the same crystal habit. For instance, all the units are polyhedral and

Downloaded from http://petrology.oxfordjournals.org/ at University of Hawaii at Manoa Library on February 13, 2013

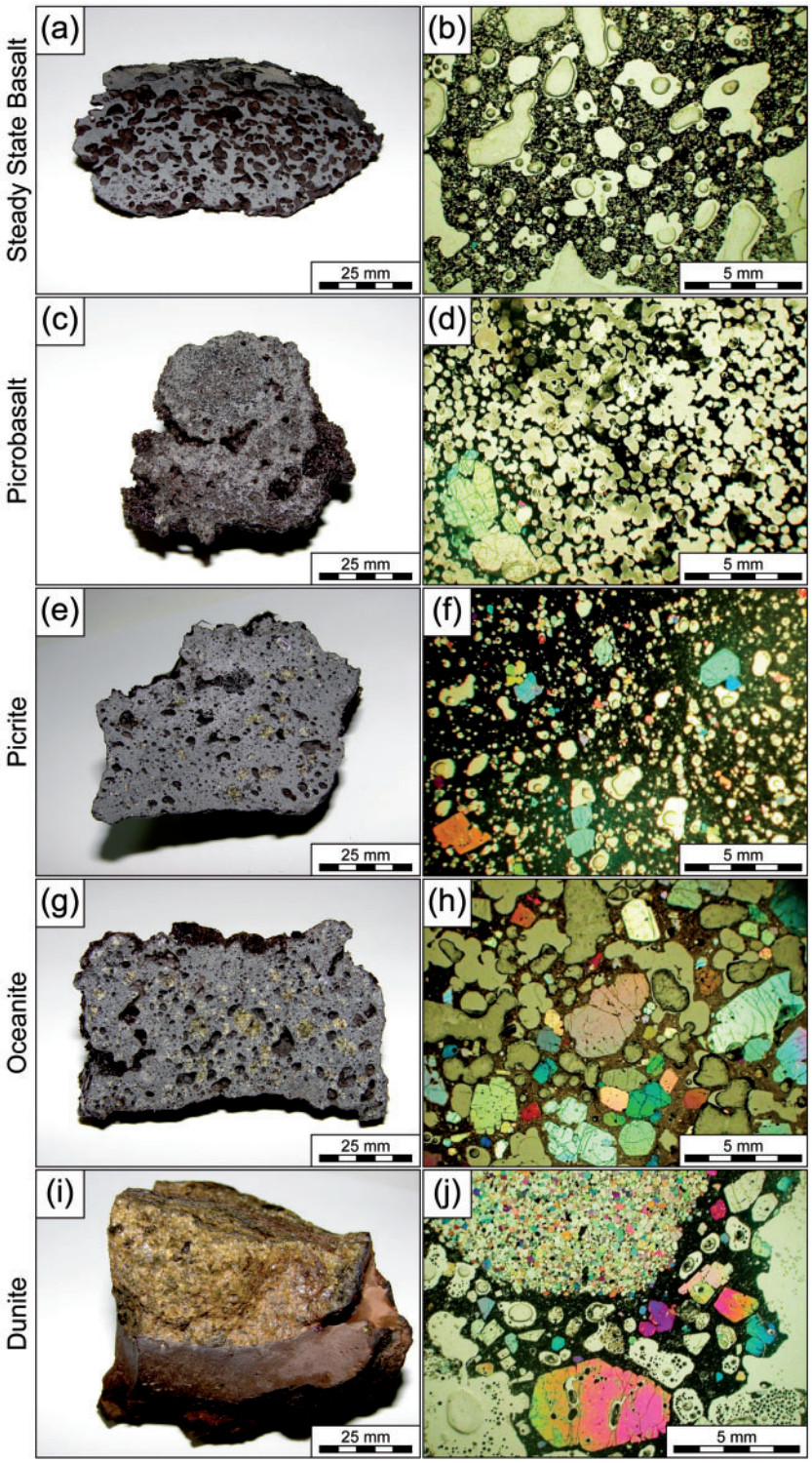

Fig. 3. Samples and rock-types of Piton de la Fournaise: (a) Steady State Basalt with 6·66 wt % MgO devoid of large olivine crystals (hand specimen sampled after natural cooling in air at day 1 of the June 2001 eruption); (b) Steady State Basalt with 7·12 wt % MgO and <5 vol. % olivine (fragment of lava flow sampled after natural cooling in air during the 1 day eruption of March 2007; transmitted-light photomicrograph with partially crossed Nicols); (c) magnesian basalt with 10·36 wt % MgO with cryptic olivine crystals (hand specimen sampled after natural cooling in air at day 2 of the January 2002 eruption); (d) magnesian basalt with 9·44 wt % MgO and ~10 vol. % olivine (fragment of lava flow collected after natural cooling at day 5 of the December 2005 eruption; transmitted-light photomicrograph with partially crossed Nicols); (e) picrite with 13·70 wt % MgO with several olivine macrocrysts (hand specimen sampled after natural cooling in air at day 5 of the January

(continued)

Downloaded from http://petrology.oxfordjournals.org/ at University of Hawaii at Manoa Library on February 13, 2013

stubby in the groups of Figs 5b, 7e and 8a–d, or polyhedral and elongated along the *a*-axis in the groups of Figs 5d and 7c and d. Similarly, all the units are skeletal and stubby in Fig. 7a, or skeletal and elongated along the *a*-axis in Fig. 6e.

Organization of crystal units. Within a single group, most of the crystal units have identical optical orientation (i.e. parallel faces, same birefringence tint and simultaneous extinction, Fig. 9a and b). Hence, all the crystal units of a group are parallel to each other (Figs 5b and d, 6e, 7–12) similar to the groupings reported by Drever & Johnston (1957). In contrast, different groups of parallel units have random orientations within the mesostasis of lava samples, and they seldom occur in contact with each other (Fig. 3c–h).

Strikingly, the parallel crystal units may display an ordered, hierarchical pattern: large units have adjacent, smaller units occurring as reduced-size replicas (i.e. with a similar shape ratio), sometimes gradually decreasing in size (Figs 8a and 9a–d). For example, the group presented in Fig. 8a is made of a chain of five parallel units with a decreasing grain size in the direction [101]. Parallel units are preferentially in contact along the *a*-axis by the interpenetration of their faces, edges and/or summits (Figs 5b, d, 6e and 7–12). Some groups contain tens of parallel units in a compact cluster, providing numerous growth faces in contact with the mesostasis (Figs 8c, d and 10). It should be noted that parallel crystal units in contact with each other in three dimensions are separated by the mesostasis in thin section, as shown in Fig. 9a, b and d. Parallel crystal units appear interpenetrated without any gap between them, yielding a large monocryst similar to olivine types [i] or [vii] (blocky and irregular crystals, and megacrysts, respectively; Supplementary Data, Appendix 1). In other words, parallel and adjacent crystal units constitute a single macrocryst (Fig. 10) rather than a cluster of aligned crystals. Because this macrocryst is composed of several units, it may display faceted cavities such as in Fig. 10a.

Misorientations. The units of a group sometimes display up to 15° misalignments in different directions (Figs 7a, b and 8a), yielding faint extinction discontinuities and slight variations in birefringence tints within the group (Fig. 10b–f). In thin section, misaligned units may have irregular contacts similar to subgrain boundaries within the group (Fig. 10b–d) but still have growth faces whenever in contact with the mesostasis. Misalignments can appear as subgrain boundaries with orientations subparallel to external growth faces (Fig. 10c and d). Undulose extinction and dislocation lamellae with less than 5° misorientation, such as those reported by Helz in olivine type [i] of blocky, irregular crystals (Supplementary Data, Appendix 1), occur preferentially in compact groups of units (Fig. 10e and f).

Twinnings. Larger misorientations of crystal units may also occur within a group (Figs 5e, 8b and 9e, f), similar to the oblique face-to-face attachments {021}–{010} and {021}–{021} observed by Schwindinger & Anderson (1989) (Supplementary Data, Appendix 2). In this case, the tilt is a 90°, 60° or 32° rotation around the *a*-axis of the crystal unit relative to the general orientation of other units, which corresponds to olivine twinnings {021}, {011} and {012}, respectively (Fig. 2). The trilling {031} was not observed in our samples. It should be noted that twins may occur between two units of the same size (Figs 5e and 9e, f). It is also important to note that units adjacent to twins copy twins' orientations (Figs 8b and 9e). As for parallel units, twins can have slight misorientations (Figs 8b and 9f).

Cleavages. Entire groups of crystal units may be cleaved along the planes (100), (010) and (001) (Fig. 8d), yielding polygonal shapes similar to olivine type [iv] of angular crystals (Supplementary Data, Appendix 1). Importantly, these cleavages invariably affect every unit placed in these planes (Fig. 2). The cleaved surfaces may be smooth or irregular and expose spinel microcrysts or cavities in the units.

Mosaicity. The final dimension of macrocrysts (i.e. each group of crystal units) has the typical shape ratio ($a:b:c = 1{\cdot}5:1:2$ in Fig. 8c) of standard, single olivine crystals (Fig. 2). Their blocky texture (Fig. 8c and d) and the frequent misorientation of their units from parallel alignment (Fig. 10b–d) are similar to the mosaic-block and lineage structure of dendrites described in metallic alloys (Buerger, 1932, 1934; Chalmers, 1964).

Zonings. Chemical maps of olivine macrocrysts display large zones depleted in P_2O_5 (<0·31 wt %) and ~10 μm

Fig. 3 Continued
2002 eruption); (f) picrite with 14·29 wt % MgO and ~21 vol. % olivine (fragment of lava flow collected after natural cooling at day 2 of the February 2005 eruption; transmitted-light photomicrograph with partially crossed Nicols); (g) oceanite with 28·13 wt % MgO and abundant olivine macrocrysts (hand specimen sampled after natural cooling in air at day 9 of the January 2002 eruption); (h) oceanite with 27·94 wt % MgO and ~53 vol. % olivine (lava sample quenched into water at day 28 of the April 2007 eruption; transmitted-light photomicrograph with partially crossed Nicols); (i) dunite enclave within host basalt (hand specimen sampled in the volcanic cone of Piton Chisny); (j) dunite enclave (top of the image) within host oceanite (xenolith found after natural cooling in air of an April 2007 lava flow; transmitted-light photomicrograph with partially crossed Nicols). The volume proportion of olivine to glassy matrix shown in (b), (d), (f) and (h) was measured using the Photoshop CS3 software. The proportion of vesicles in each lava sample is dependent on the sampling method.

Downloaded from http://petrology.oxfordjournals.org/ at University of Hawaii at Manoa Library on February 13, 2013

Table 2: Representative composition of olivine and associated phases

Oxide	Olivine									Cr-spinel			Glass				
(wt %)	Mesocryst		Macrocryst					d.l.	uncert.	Inclusion	d.l.	uncert.	Melt inclusion		Matrix	d.l.	uncert.
	core	edge	core	edge	P-rich zones	P-rich zones	P-rich zones	av.	av.		av.	av.	Primary	Secondary		av.	av.
SiO_2	39·28	39·74	39·98	39·41	39·96	40·39	40·24	0·14	0·34	0·07	0·14	0·03	49·59	49·88	50·18	0·13	0·47
Al_2O_3	0·00	0·03	0·05	0·00	0·00	0·00	0·00	0·18	0·04	17·59	0·13	0·25	15·57	15·42	13·86	0·19	0·34
FeO_t	16·53	18·96	14·78	20·18	15·24	14·47	14·97	0·27	0·69	29·52	0·30	1·11	9·32	8·56	10·99	0·26	0·55
MnO	0·31	0·25	0·15	0·31	0·21	0·21	0·22	0·18	0·11	0·31	0·24	0·14	0·23	0·15	0·19	0·24	0·13
MgO	44·27	41·25	45·28	40·94	44·64	45·21	44·95	0·11	0·51	11·57	0·09	0·21	6·40	5·81	6·11	0·08	0·11
CaO	0·35	0·36	0·30	0·44	0·24	0·20	0·26	0·09	0·05	0·14	0·09	0·04	11·97	11·38	10·93	0·10	0·31
Na_2O	0·00	0·02	0·02	0·03	0·00	0·06	0·00	0·11	0·05	0·03	0·12	0·06	2·88	3·23	2·81	0·10	0·16
K_2O	0·01	0·00	0·00	0·02	0·00	0·00	0·00	0·08	0·05	0·00	0·09	0·05	0·80	0·62	0·82	0·08	0·10
TiO_2	0·00	0·04	0·02	0·06	0·00	0·03	0·00	0·05	0·01	4·36	0·05	0·04	2·42	2·90	3·30	0·05	0·05
P_2O_5	0·04	0·02	0·02	0·00	1·01	0·51	0·63	0·14	0·02	0·01	0·13	0·02	0·21	0·23	0·34	0·19	0·03
NiO	0·20	0·27	0·46	0·21	0·25	0·26	0·25	0·22	0·13	0·13	0·31	0·17	0·05	0·00	0·00	0·29	0·15
Cr_2O_3	0·01	0·01	0·03	0·03	0·04	0·05	0·00	0·05	0·02	33·50	0·07	0·21	0·15	0·02	0·02	0·07	0·03
Total	101·00	100·96	101·08	101·62	101·58	101·39	101·53			97·23			99·57	98·21	99·56		
Fo*	Fo82·7	Fo79·5	Fo84·5	Fo78·3	Fo83·9	Fo84·8	Fo84·3										
K_D†	$0{\cdot}23_{matrix}$	$0{\cdot}28_{matrix}$	$0{\cdot}20_{matrix}$	$0{\cdot}30_{matrix}$	$0{\cdot}21_{matrix}$	$0{\cdot}20_{matrix}$	$0{\cdot}21_{matrix}$						$0{\cdot}25_{core}$	$0{\cdot}25_{core}$			

Data are from day 19 of April 2007 eruption, except for the mesocryst, which comes from a day 4 sample, and P-rich zonings in macrocrysts which come from samples taken at day 24 of the December 2005 eruption—all these samples are oceanites quenched in water). The compositions of olivine edges were obtained from spots at a distance <10 μm from the border of crystals.
d.l., detection limit; av., average; uncert., uncertainty.
*Forsterite content $Fo = 100\,Mg/(Mg + Fe_t)$.

†Distribution coefficient $K_D = \frac{(MgO/FeO_t)_{Liq}}{(MgO/FeO_t)_{Olivine}}$ (Toplis, 2005) between olivine and the uniform matrix glass or the melt inclusion.

Downloaded from http://petrology.oxfordjournals.org/ at University of Hawaii at Manoa Library on February 13, 2013

Table 3: List of olivine textures observed in the figures

Texture	Figure
Habit of units	
Polyhedral	5, 6f, 7b–e, 8–12
Skeletal (hopper cavities)	6a–d, 7a, b
Elongation along the *a*-axis	5c, d, 6d, e, 7c, d
Organization of units	
Parallel pattern	5b, d, 6e, 7–10, 11a, d, e, 12
Hierarchization	8a, 9a–d
Mosaicity	8c, d, 10a–f
Misorientation	7a, b, 8a
Subgrain boundary	10b–d
Dislocation plane	10e, f
Twinning	
021	5e, 8b, 9e
011	9f
012	3d
Cleavage	8d
Shape of melt inclusions	
Ovoid	7a–e, 11c–e
Negative crystal	11f
Elongated	7c
Cr-spinel inclusion	9a–f, 10b–f, 11a–d

thick zones enriched in P_2O_5 (0·41–1·01 wt %, Table 2, Fig. 12a and b). Faint zoning in Cr and Al is also detected in superimposition with the P-rich zone, as observed by Milman-Barris *et al.* (2008). Each crystal unit of a given macrocryst (i.e. group) has at least one rim enriched in P_2O_5 near the edges in contact with the mesostasis. When the section is cut in the plane (001), P-, Cr- and Al-rich zones may also occur as concentric 'oscillatory zoning' (Fig. 12a) or at the centre of a crystal unit (Fig. 12b and c). These zonings are parallel to external forms {010}, {110} and {120}. The 'herring-bone' zoning of the literature (figs 1a, e, 2a and 3e, f of Milman-Barris *et al.*, 2008) was not observed in our chemical maps in the sections (100), (010) and (001).

Inclusions. The crystal units of olivine macrocrysts contain various amounts of spinel microcrysts (ø < 100 μm), large melt inclusions (ø 10–200 μm) and planes of small melt inclusions (ø < 10 μm, Fig. 11a–f). Olivine is the only mineral to trap spinel microcrysts (i.e. there is no spinel in clinopyroxene and plagioclase) and spinel is the only mineral trapped as solid inclusions in olivine. Spinel is also absent from the mesostasis of water-quenched samples (Welsch *et al.*, 2009). Spinel microcrysts have a cubic or octahedral habit and occur as crystal inclusions often associated with melt inclusions (Fig. 11d) or olivine embayments (Fig. 11c). In the first case, olivine is cracked around the spinel microcryst inclusions (Fig. 11b). Planes of small melt inclusions may be oriented randomly in the crystal or disposed parallel to the external faces (Fig. 11e and f). Most melt inclusions have an ovoid shape with a shrinkage bubble (Fig. 11f). They can also be elongated (Fig. 7c) or faceted into a negative crystal of olivine with orientations parallel to the external faces of the host crystal (Fig. 11f). Importantly, the form {021} of polyhedral units can have a central cavity opened to the mesostasis (Fig. 7e, unit 1), or enclosed within a large melt inclusion (Fig. 7e, unit 2). This cavity occurs at the same location as that of the cavity faceted in an 'amphitheatre' within the skeletal units (Figs 6a–c and 7a, b). Sulphide globules may occur alone in olivine crystals or as a separate phase in melt inclusions, as in olivine type [v] of the literature (euhedral crystal containing sulphide inclusions; Supplementary Data, Appendix 1). Sulphide globules contain 590–1745 ppm sulphur (Bureau *et al.*, 1998*b*). Similar inclusions have been described in other settings such as Stromboli (Métrich *et al.*, 2010), the East Pacific Rise, Iceland (Roeder *et al.*, 2001), Hawaii (Roeder *et al.*, 2003) and the Mid-Atlantic Ridge (Schiano, 2003).

Mesocrysts in lavas

Despite their variable abundance in the 2002–2007 lavas, olivine mesocrysts have textures similar to those described by Welsch *et al.* (2009). They are polyhedral (Fig. 13a) or skeletal (i.e. polygonal with faceted cavities) with occasional 50–200 μm long dendritic overgrowths (Fig. 13b). They often occur as clusters of several grains in contact with each other or with interstitial glass. The various extinction angles and birefringence tints of the olivine mesocrysts, similar to the dunitic type [vi] described by Helz (1987; Supplementary Data, Appendix 1), indicate that these crystals are randomly oriented in the clusters (i.e. no synneusis attachment: Supplementary Data, Appendix 2). Olivine mesocrysts do not show evidence of intracrystalline deformation. They may contain euhedral spinel microcrysts and ovoid or faceted melt inclusions with a shrinkage bubble.

Dunites in lavas and lapilli

The dunite samples from Piton Chisny, Piton Caille and the April 2007 lavas have textures similar to the olivine type [vi] in dunitic aggregates reported by Helz (1987) in the 1959 picrite at Kilauea Iki (Supplementary Data, Appendix 1). Dunites are dense clusters of olivine crystals with a large range of grain sizes (0·1–1 mm), joined together with a few remaining interstices (Fig. 14a–f). Olivine crystals are anhedral: they have asymmetric shapes and their faces are dictated by the contact of grains, not by growth shapes freely developed in the melt (Fig. 14a–d). Olivine grains have various birefringence tints and extinction angles,

Downloaded from http://petrology.oxfordjournals.org/ at University of Hawaii at Manoa Library on February 13, 2013

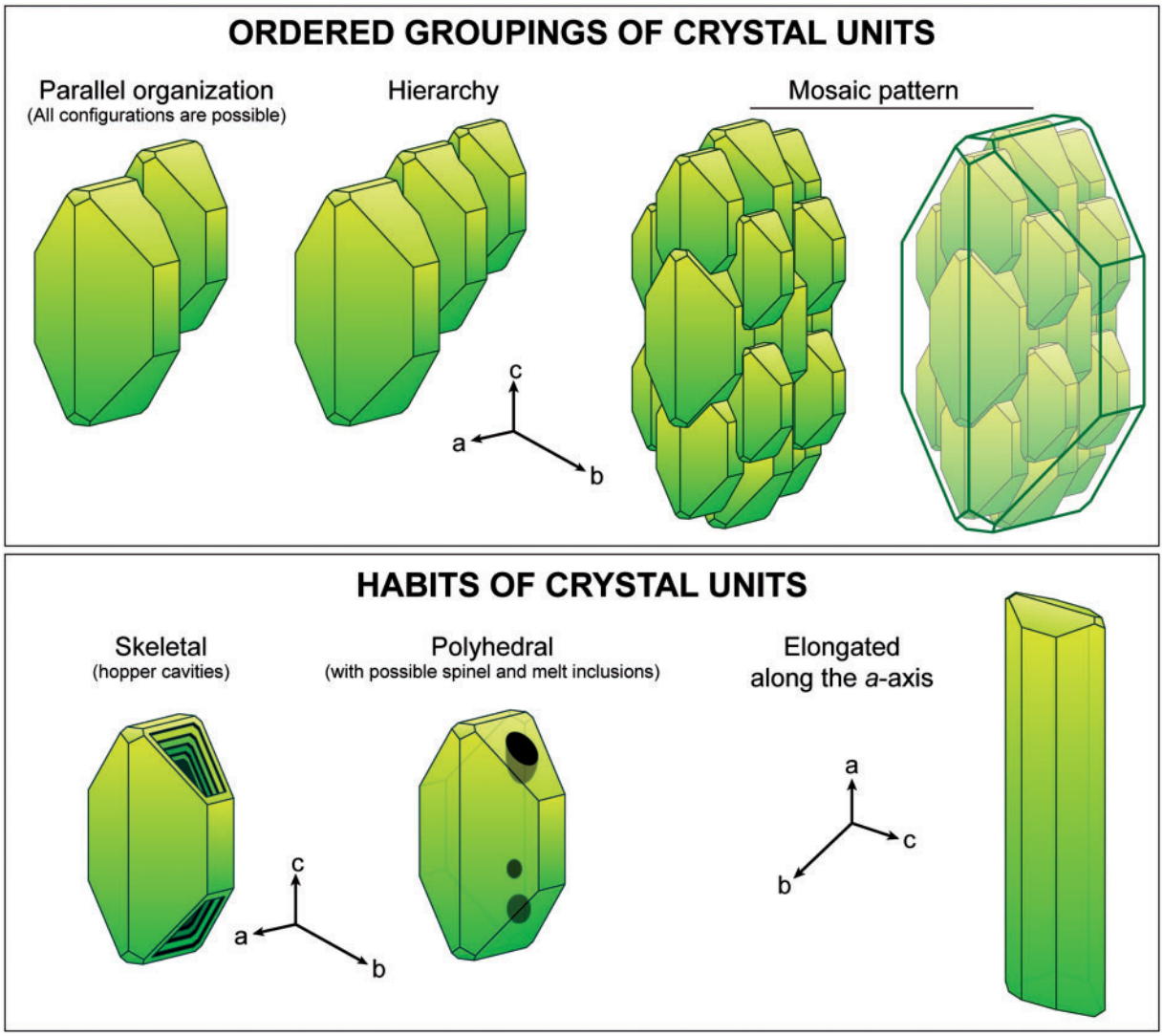

Fig. 4. Main textures of olivine macrocrysts. The sketch of crystal units in the parallel groupings has been drawn from unit 2 in Fig. 7e with a shape ratio of $a:b:c = 1{\cdot}1:2{\cdot}2:2{\cdot}2$ using central distances at {010} 0·61, {110} 0·43, {021} 0·71, {101} 0·92 and {001} 1·00. The model for the unit elongated along the *a*-axis is the large unit in Fig. 7d with a shape ratio of $a:b:c = 6{\cdot}6:1{\cdot}1:1{\cdot}7$ using central distances at {010} 0·12, {110} 0·78, {021} 0·14 and {101} 0·78.

indicating random orientations. They have occasional undulose extinction or dislocation lamellae (Fig. 14c and d) similar to those observed in olivine macrocrysts (Fig. 10e and f). One dunite sample from Piton Caille has been found to contain groups of parallel crystal units (Fig. 14e and f) similar to those observed in olivine macrocrysts (Fig. 8c and d). Large olivine grains may even contain ovoid melt inclusions and euhedral spinel microcrysts like those of olivine macrocrysts (Fig. 11).

DISCUSSION

Mechanisms of olivine association

The first step in the interpretation of olivine shapes is to understand how macrocrysts form. The organized subdivision of macrocrysts in subparallel units (Figs 5–12) indicates that the assemblage process is highly selective with regard to the crystallographic orientations of the units, which excludes a random aggregation of separated crystals. This systematic pattern, and the close connection between crystal units (e.g. Figs 7e and 8a) cannot be explained by either the aggregation of multiple nuclei through heterogeneous nucleation or parallel growth, because the growth of each nucleus would result in superimposition leading to a single crystal (Supplementary Data, Appendix 3). There are also probabilistic arguments against synneusis as a likely mechanism of crystal unit organization (Supplementary Data, Appendix 2; see also Dowty, 1980*b*). Indeed, if all the faces have an equal probability of attaching another crystal in parallel, then the

Downloaded from http://petrology.oxfordjournals.org/ at University of Hawaii at Manoa Library on February 13, 2013

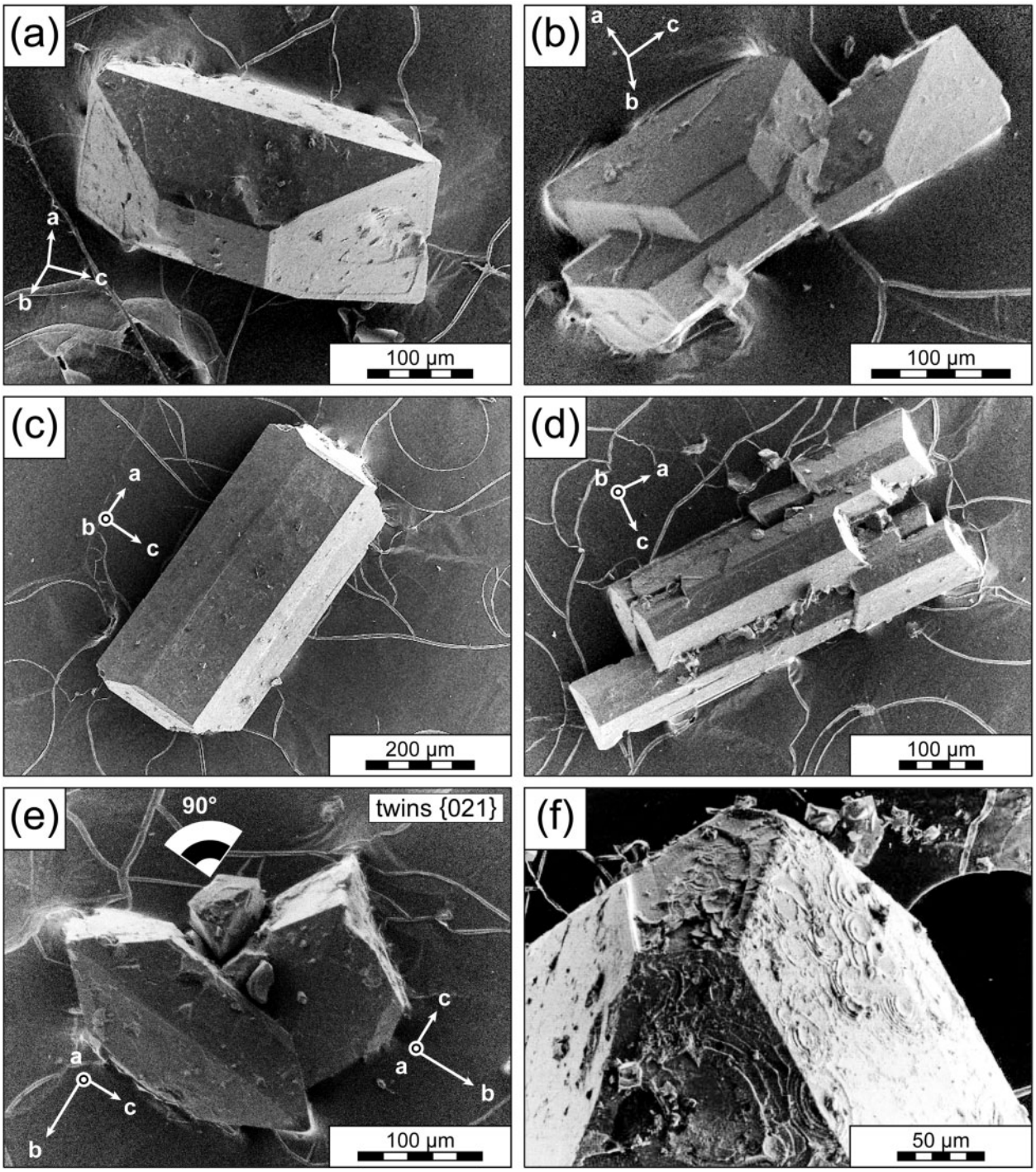

Fig. 5. SEM images of mesostasis-free macrocrysts from Piton Caille: (a) single crystal showing external growth faces; (b) parallel group of three faceted crystal units (note the similar crystal habit of the three units); (c) single, well-faceted crystal elongated along the *a*-axis; (d) parallel group of seven faceted crystal units showing a crystal habit elongated along the *a*-axis; (e) twins {021}; (f) surface of a polyhedral crystal showing concentric circles of glass. These relics indicate the growth of gas bubbles at the contact with olivine (presumably during magma ascent) without any significant modification of the polyhedral habit.

Downloaded from http://petrology.oxfordjournals.org/ at University of Hawaii at Manoa Library on February 13, 2013

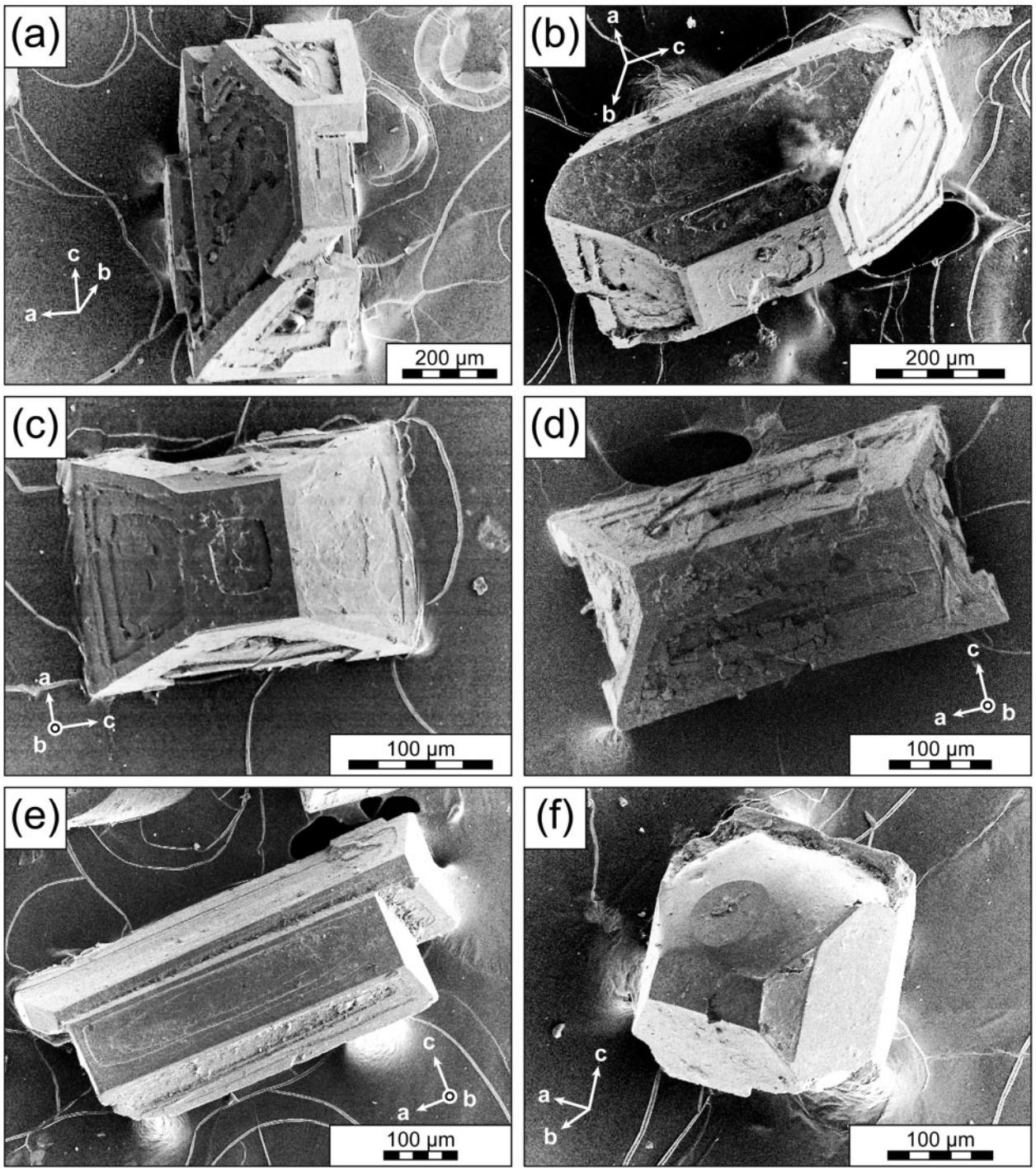

Fig. 6. SEM images of mesostasis-free macrocrysts from Piton Caille: (a–c) skeletal crystals showing different growth steps (note that their hollow faces are made of concentric terraces); (d, e) skeletal crystals elongated along the *a*-axis [note the similar crystal habit of the two units in (e)]; (f) well-faceted crystal with a circular depression showing the remnants of a hollow face (021).

probability of attaching five crystals (eight pairs of parallel faces each) in a linear array such as in Fig. 8a is $1/8^5$. The probability of attaching these five aligned crystals in a decreasing size order is $1/8^5 \times ½^3$ or 0·0004%, making the group in Fig. 8a almost impossible to obtain. The same reasoning may apply to the three ordered groups shown in Fig. 9a–d, and also to Hawaiian olivine (e.g. fig. 2a of Vinet & Higgins, 2010). Conversely, if the faces

Downloaded from http://petrology.oxfordjournals.org/ at University of Hawaii at Manoa Library on February 13, 2013

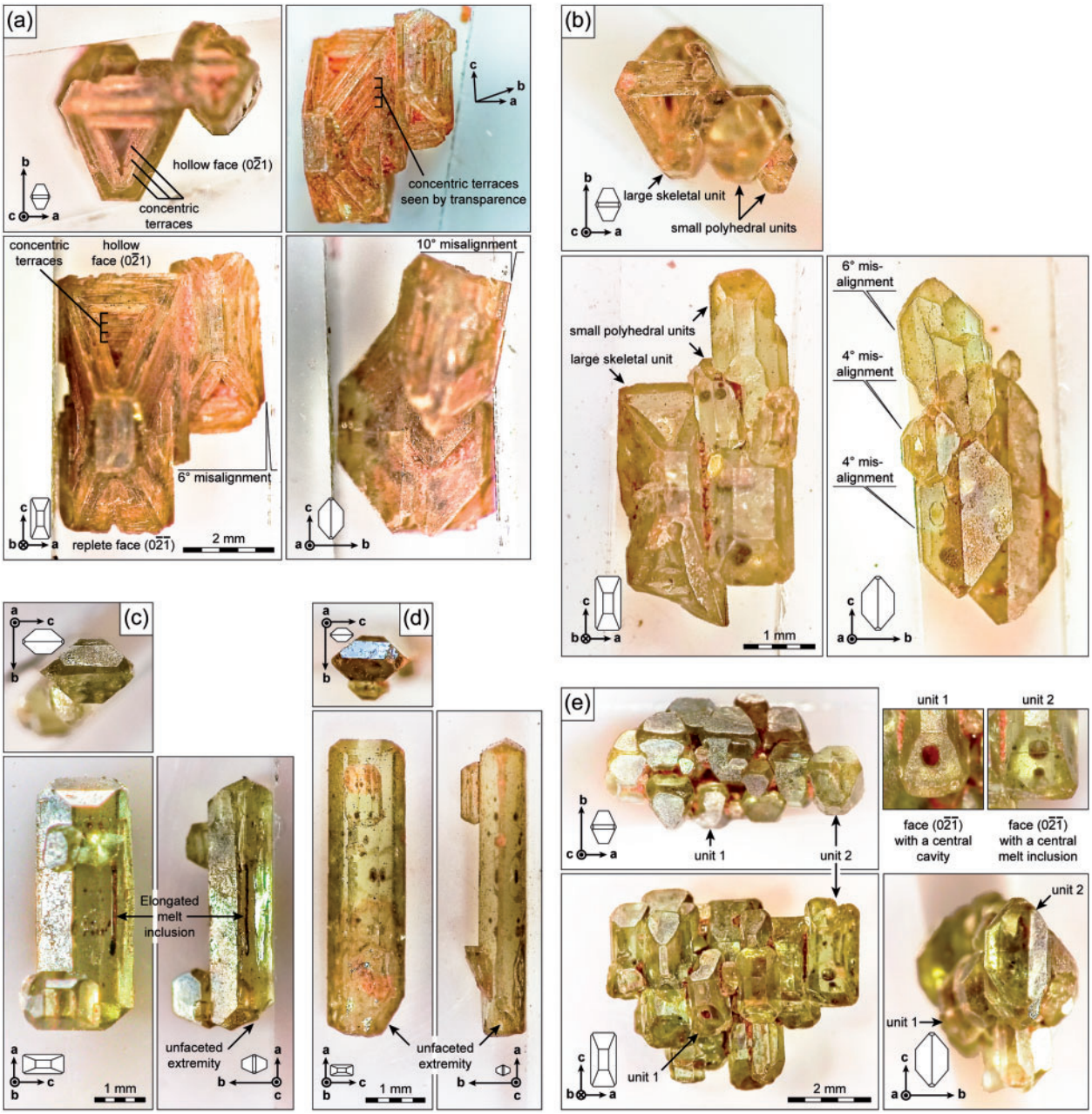

Fig. 7. Textures of mesostasis-free olivine macrocrysts from Piton Caille (each macrocryst was photographed with a stereomicroscope in the three directions). (a) Parallel grouping of two skeletal units with slight misalignment and conchoidal fractures. Units have characteristic hollow forms {021} built up on the interlocking of concentric terraces. (b) Parallel grouping made of one large skeletal unit (with basal conchoidal fracture) and several small polyhedral units. (c) Parallel grouping composed of one large unit elongated along the *a*-axis with smaller units. It should be noted that the largest unit shows a melt inclusion elongated along the *a*-axis and an unfaceted extremity. (d) Parallel grouping made of one large unit elongated along the *a*-axis and smaller units. The unfaceted extremity of the largest unit should be noted. (e) Parallel grouping of 20 polyhedral units. Unit 1 has a face (0 $\bar{2}$ $\bar{1}$) with a central cavity open to the exterior. Unit 2 has a face (0 $\bar{2}$ $\bar{1}$) with a central cavity enclosed within a melt inclusion.

do not have an equal probability of attachment, then large groups containing tens of units should systemically grow in the direction perpendicular to the faces having the highest probability of attachment, which is not the case (mosaic crystals of Fig. 8c and d).

Alternatively, we propose that the organized subdivision of macrocrysts in subparallel units (Figs 5–12) is the result of dendritic growth. A dendrite is a branching structure with uniform lattice and optical properties resulting from the extension of a single crystal in preferred growth

Downloaded from http://petrology.oxfordjournals.org/ at University of Hawaii at Manoa Library on February 13, 2013

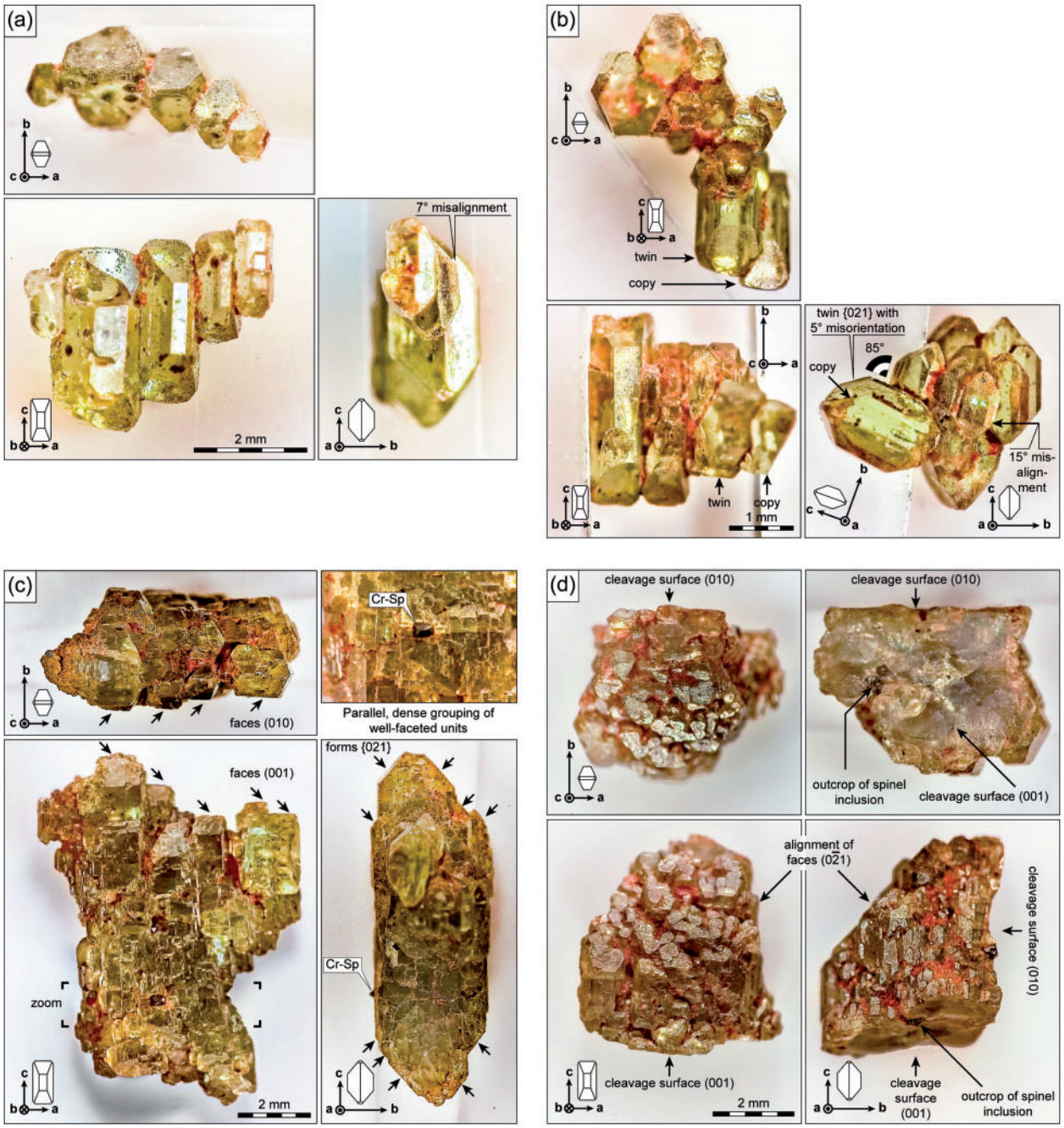

Fig. 8. Textures of mesostasis-free olivine macrocrysts from Piton Caille (each macrocryst was photographed with a stereomicroscope in the three directions). (a) Parallel grouping of five polyhedral units. Note that four of these units are perfectly ordered by decreasing grain size along the direction [10$\bar{1}$]. Note also the slight misalignment of one unit. (b) Parallel grouping containing a misoriented twin {02$\bar{1}$}. Note that the twin has an adjacent unit with the same crystallographic orientation. (c) Parallel grouping formed of tens of tiny units densely assembled. It should be noted that the group has a whole shape similar to the polyhedral habit of olivine, yielding a mosaic texture. (d) Parallel grouping formed of tens of tiny units densely assembled. It should be noted that cleavages (010) and (00$\bar{1}$) affect indistinctly every unit placed in the plane of cut. Cleavages also make spinel inclusions crop out.

directions (Cody & Cody, 1995). Observed at various scales, an olivine dendrite is made of several skeletal crystal units with identical orientations (Donaldson, 1976; Faure *et al.*, 2003*a*, 2003*b*). The crystal units are replicas that may be disposed into a column along the *a*-axis, forming an elongated crystal similar to the olivine macrocrysts shown in Figs 5c, d, 6d, e and 7c, d. Crystal units may also be disposed into a chain as observed in Figs 5b, d, 6e

Downloaded from http://petrology.oxfordjournals.org/ at University of Hawaii at Manoa Library on February 13, 2013

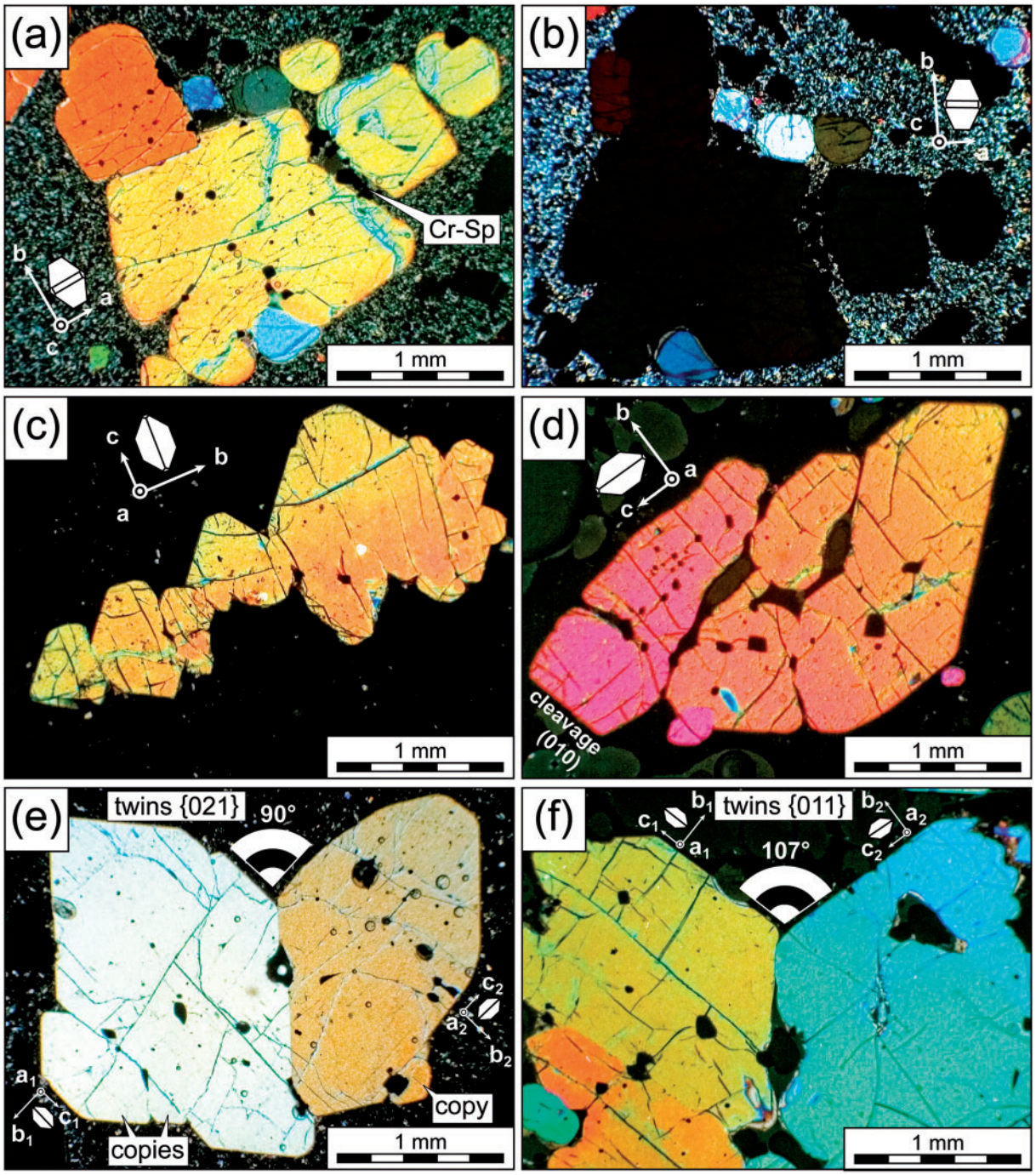

Fig. 9. Textures of olivine macrocrysts in thin sections of recent lava flows at Piton de la Fournaise (transmitted-light photomicrographs with crossed Nicols). (a) Parallel group of polyhedral units. It should be noted that the parallel units have continuous birefringence tints and rounded edges in contact with the crystallized mesostasis. Also noteworthy is the occurrence of spinel microcrysts at the junction of, or within, the units (air-cooled sample of February 2005 eruption). (b) Same as (a) but with a 45° rotation of the plate, showing the simultaneous extinction of most crystal units. (c) Parallel grouping of four crystal units ordered with a decreasing grain size along the direction [0l0] (lava sample quenched into water at day 24 of the December 2005 eruption). (d) Parallel grouping of three polyhedral units also showing a hierarchical organization. The units have continuous optical properties even when separated by the mesostasis. The spinel inclusions aligned in a direction parallel to the external faces of the olivine crystal should be noted (lava sample quenched into water at day 7 of the April 2007 eruption). (e) Crystal twins {021}. The small adjacent units copying the orientations of crystal twins should be noted. The cavities devoid of mesostasis are caused by thin section preparation (lava sample quenched into water at day 9 of the February 2005 eruption). (f) Crystals twins {011} with 13° misorientation. The cavities devoid of mesostasis are due to thin section preparation (lava sample quenched into water at day 24 of the December 2005 eruption).

Downloaded from http://petrology.oxfordjournals.org/ at University of Hawaii at Manoa Library on February 13, 2013

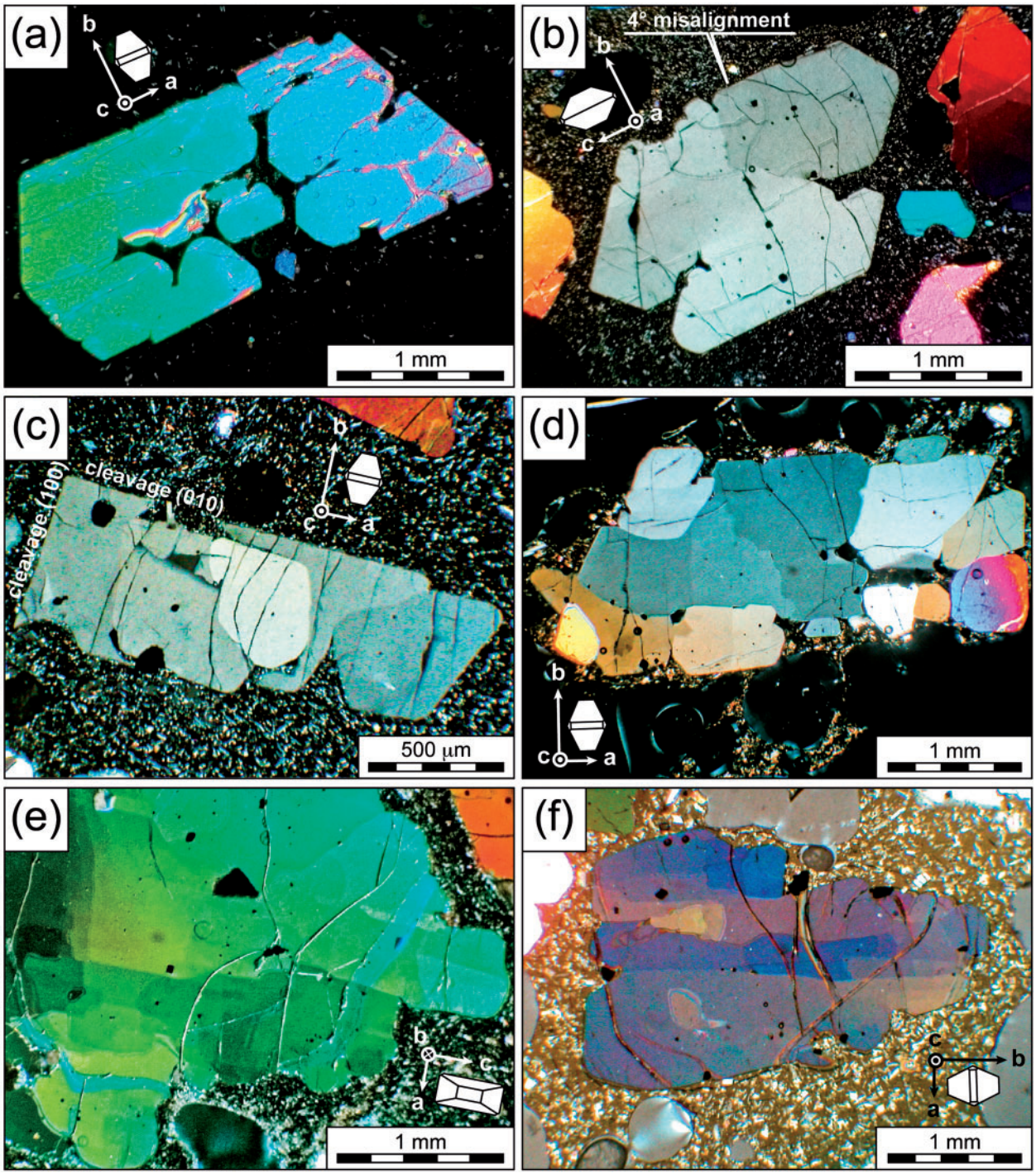

Fig. 10. Textures of olivine macrocrysts in thin sections of recent lava flows (transmitted-light photomicrographs with crossed Nicols). (a) Parallel grouping of several small crystal units forming a large monocrystal with faceted cavities (lava sample quenched into water at day 24 of the December 2005 eruption). (b) Parallel grouping of three units, one of which is misoriented with respect to the two other units (lava sample quenched into water at day 6 of the April 2007 eruption). (c) Parallel grouping formed with several misaligned units. It should be noted that their subgrain boundaries may be curved or parallel to the external faces (lava sample quenched into water at day 6 of the April 2007 eruption). (d) Large parallel grouping containing several misaligned units. It should be noted that some subgrain boundaries are parallel to the external faces (lava sample quenched into water at day 27 of the April 2007 eruption). (e) Large parallel grouping containing several irregular dislocation planes (lava sample quenched into water at day 6 of the April 2007 eruption). (f) Parallel grouping showing dislocation lamellae (lava sample quenched into water at day 28 of the April 2007 eruption).

Downloaded from http://petrology.oxfordjournals.org/ at University of Hawaii at Manoa Library on February 13, 2013

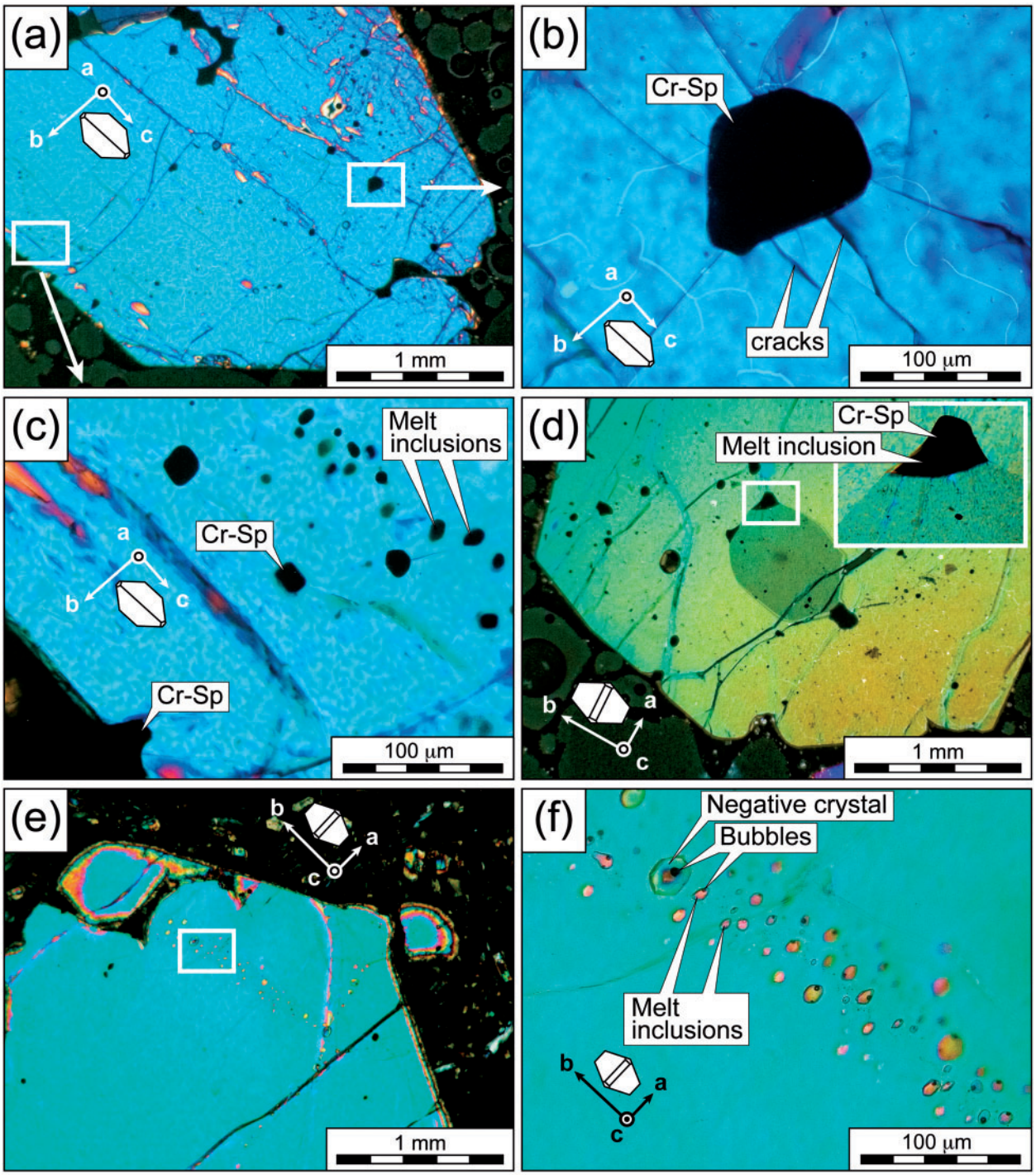

Fig. 11. Inclusions in olivine macrocrysts observed in thin sections of recent lava flows (transmitted-light photomicrographs with crossed Nicols). (a) Macrocryst with spinel and melt inclusions. The alignment of the inclusions parallel to the faces of the host crystal should be noted (lava sample quenched into water at day 24 of the December 2005 eruption). (b) Cr-spinel inclusion with radial cracks in the host olivine. (c) Cr-spinel inclusions with a plane of small melt inclusions. (d) Well-faceted macrocryst enclosing a rounded unit (misorientation within 5°). The position and the shape of the melt inclusion associated with the Cr-spinel should be noted (lava sample quenched into water at day 24 of the December 2005 eruption). (e) Plane of small melt inclusions (lava sample quenched into water at day 24 of the December 2005 eruption). (f) Small melt inclusions containing a shrinkage bubble. Melt inclusions are ovoid or faceted into a negative crystal, the orientation of which is identical to that of the host macrocryst. Mineral abbreviations are after Kretz (1983).

Downloaded from http://petrology.oxfordjournals.org/ at University of Hawaii at Manoa Library on February 13, 2013

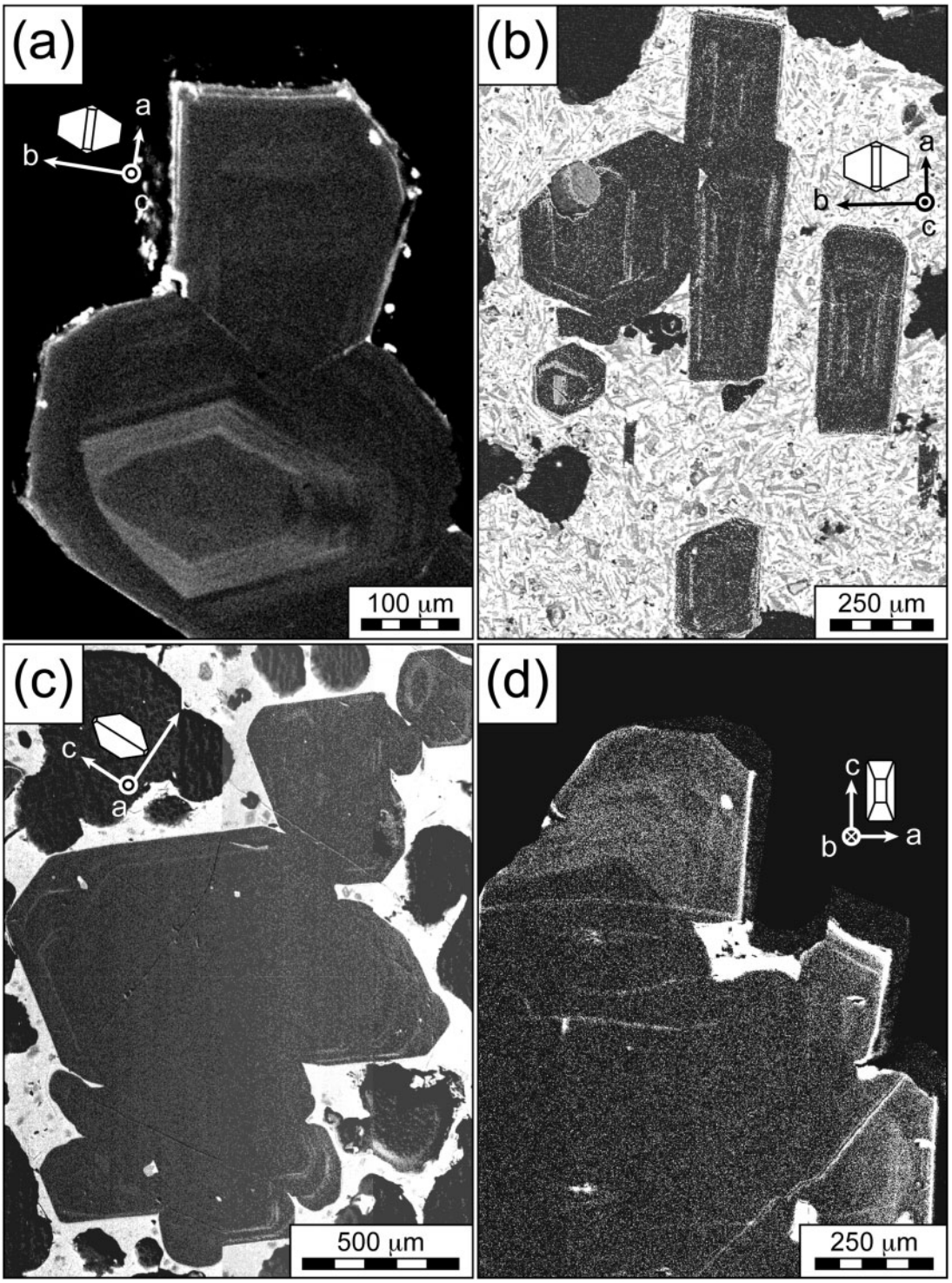

Fig. 12. Distribution of P in olivine macrocrysts. (a) Oscillatory pattern made of concentric P-rich zones parallel to the external faces. The intergrowth between the two units indicates their co-crystallization. It should be noted that the upper unit shows no oscillatory zoning in this section (mesostasis-free macrocryst from Piton Caille). (b) Skeletal patterns. The re-entrant P-rich zones in the direction [100] of the units should be noted. The units sometimes have a first zoning located at the core and usually a second one located at the quasi-contact with rims (lava sample quenched into water at day 10 of the February 2005 eruption). (c) Double zoning near the borders of each crystal unit indicating their mutual growth history. The absence of zoning at the junction of the units should be noted (lava sample quenched into water at day 24 of the December 2005 eruption). (d) Blurry zoning. The core of the group is more depleted in P than its rim (mesostasis-free macrocryst from Piton Caille).

Downloaded from http://petrology.oxfordjournals.org/ at University of Hawaii at Manoa Library on February 13, 2013

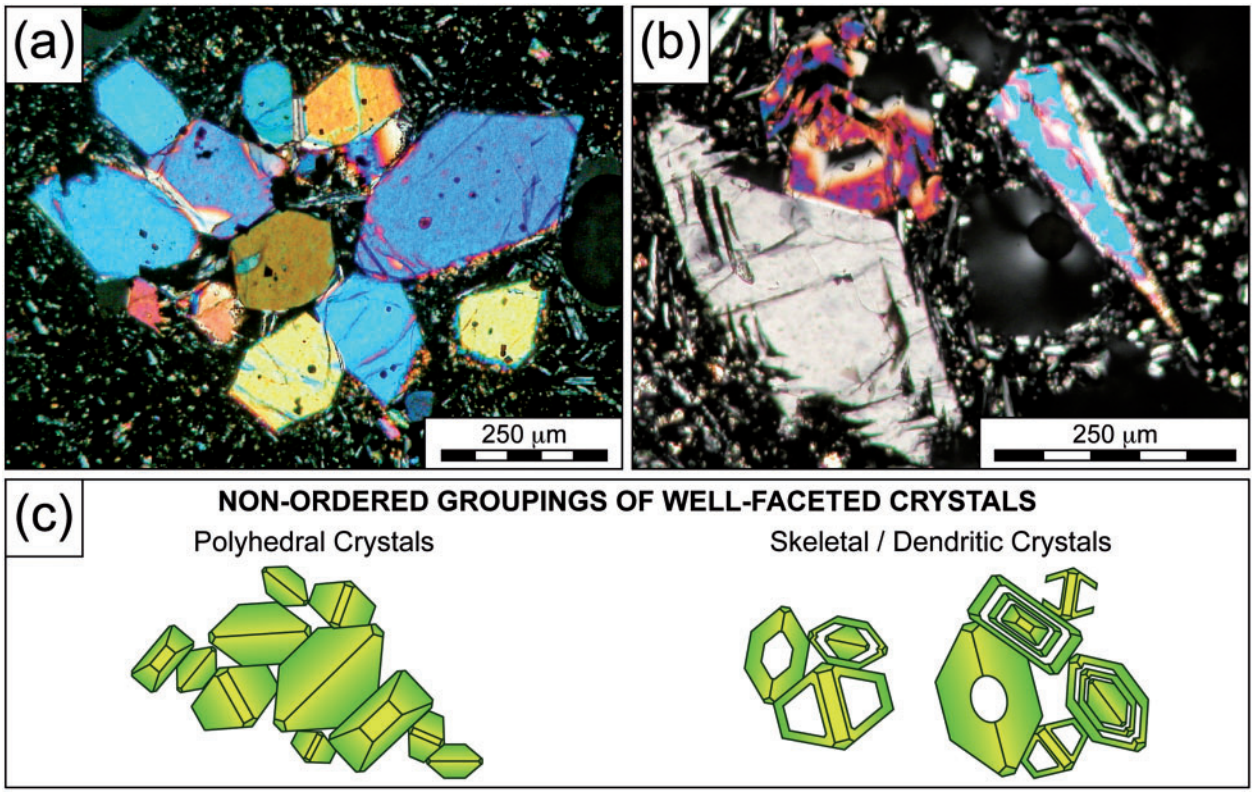

Fig. 13. Textures of olivine mesocrysts. (a) Cluster of polyhedral crystals. The random orientation of crystals and the occurrence of interstitial groundmass in the cluster should be noted (lava sample quenched into water at day 2 of the February 2005 eruption; transmitted light photomicrograph with crossed Nicols). (b) Cluster of dendritic crystals (lava sample cooled in air at day 5 of the December 2005 eruption; transmitted light photomicrograph with crossed Nicols). (c) Summary sketch of olivine mesocryst clusters.

and 7–12. The dendritic nature of olivine macrocrysts is evidenced from their ordered organization with a decreasing grain size (Figs 8a and 9a–d) and the skeletal shape of their units (Figs 6 and 7a, b), also fossilized by their melt inclusions (Fig. 7e, unit 1). The existence of a single atomic lattice in each group is indicated by the identical orientation of units, their identical optical properties and their continuous contacts (Figs 9 and 10). Hence, olivine macrocrysts are not crystal aggregates, but large monocrysts made of several buds (Wadsworth, 1961). In other words, each parallel unit of a given group is a subcrystal deriving from the splitting growth of the same lattice (Faure *et al.*, 2003*b*). Evidence for this is provided by the fact that each group of parallel units has a shape similar to a single olivine crystal (Figs 8c and 10a, b), and that cleavages propagate from one crystal unit to another within the same group (Fig. 8d). Moreover, the fact that all the units of a given group have a similar crystal habit (e.g. Figs 5b, d, 6e and 7a) implies that these units have grown under the same physico-chemical conditions.

It is also important to note that the pairs of units combined with a 90°, 60° or 32° rotation around the *a*-axis (Figs 5e, 8b and 9e, f) are not crystals aggregated with the dendrite, but twins grown from the same lattice. Twins also have smaller, parallel crystal units copying their orientation (Figs 8b and 9e), which indicates that the dendritic growth of olivine propagated throughout the twinned units. Because buds and twins may show similar grain sizes (Fig. 9e and f), the crystallization of twins is probably simultaneous with that of dendrite units. We therefore suggest that olivine twinning is not due to mineral deformation (solid-state glide) or transformation (changing mineral structure with pressure or temperature variations), but is due to growth accidents (i.e. lattice mistakes in the stacking sequence) that happened during the early steps of olivine crystallization under conditions of high supersaturation (Buerger, 1945).

In contrast to the ordered pattern of macrocrysts, the random organization of olivine mesocryst clusters (Fig. 13) suggests that these crystals nucleated separately in the magma and were attached subsequently by intergrowth. Olivine crystals in dunite samples show similar non-ordered dispositions (Fig. 14a–d) to olivine mesocrysts, suggesting that these crystals also nucleated as separate entities before aggregation. None the less, the granular shape of olivine (i.e. the absence of crystallographic contours) and the absence of significant porosity in dunitic fabrics suggest that these crystals accumulated in a storage

Downloaded from http://petrology.oxfordjournals.org/ at University of Hawaii at Manoa Library on February 13, 2013

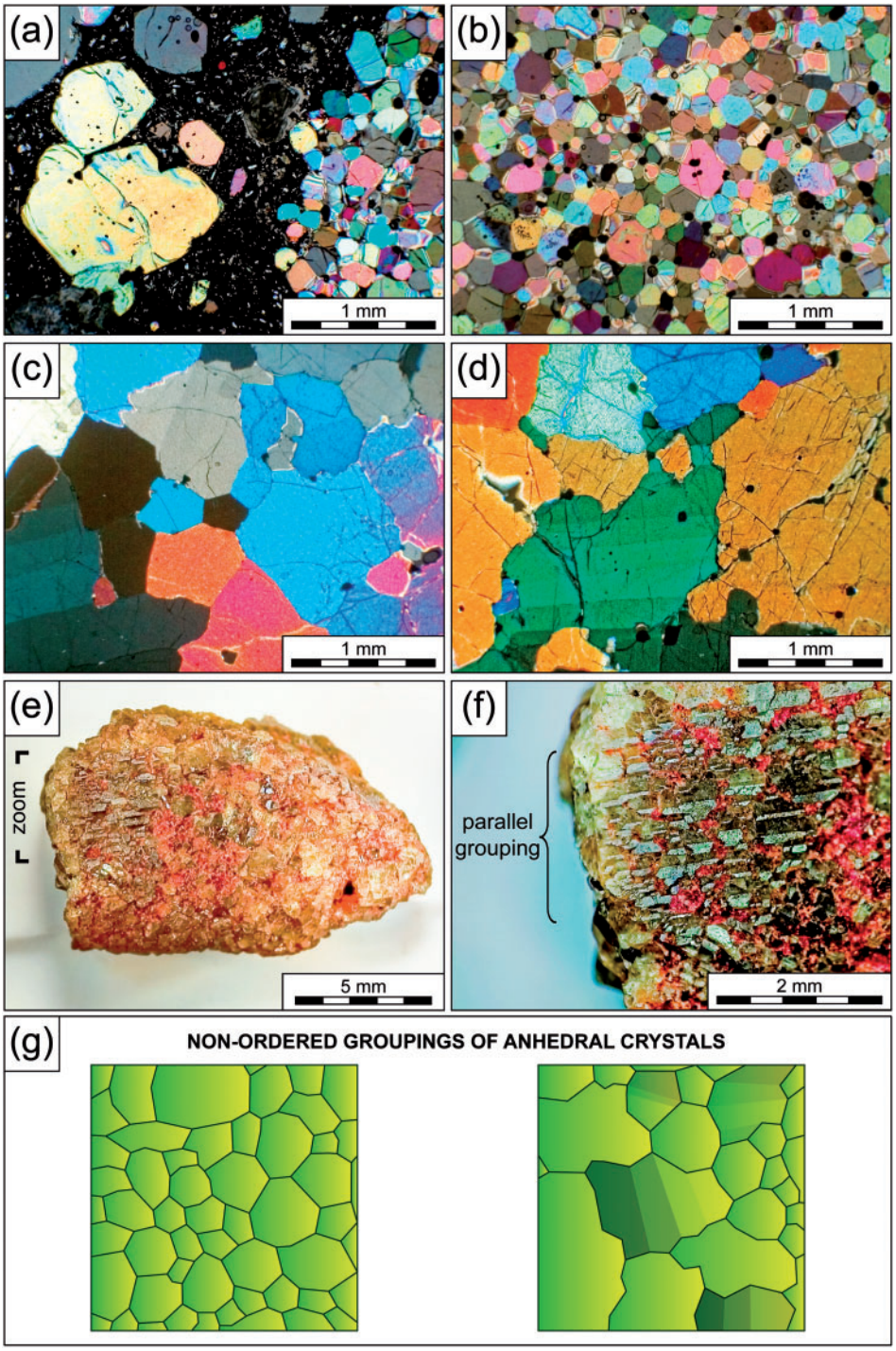

Fig. 14. Textures of dunite enclaves. (a) Textural differences between olivine grains of dunite (right side) and olivine macrocrysts of oceanite (left side) (xenolith found after activity in lava flows of April 2007; transmitted-light photomicrograph with crossed Nicols). (b) Non-ordered packing of small granular crystals containing Cr-spinel and melt inclusions [same enclave as (a); transmitted-light photomicrograph with crossed Nicols]. (c) Non-ordered packing of large and small granular crystals. The occurrence of dislocation lamellae in the grain on the left should be noted (xenolith found in the volcanic area of Piton Chisny; transmitted-light photomicrograph with crossed Nicols). (d) Non-ordered packing of large granular crystals. The occurrence of dislocation lamellae in the lower grain should be noted (xenolith found in the volcanic area of Piton Chisny; transmitted-light photomicrograph with crossed Nicols). (e) Non-ordered packing of olivine crystals containing a parallel grouping of units (fragments of dunite found in Piton Caille scoria; photomicrograph with stereomicroscope). (f) Dense parallel grouping (similar to olivine macrocrysts in Fig. 8c and d, also sketched in Fig. 4—mosaic pattern) enclosed in a non-ordered packing of granular crystals (photomicrograph with stereomicroscope). (g) Summary sketches of dunitic textures.

Downloaded from http://petrology.oxfordjournals.org/ at University of Hawaii at Manoa Library on February 13, 2013

zone, then filled the intergranular space by expelling the interstitial liquid during the course of their growth (e.g. Wager *et al.*, 1960). This step of maturation and consolidation (transforming the crystal packing into a solid fabric) may be caused by dissolution–recrystallization processes through the load and compaction of crystals, and/or by the pervasive crystallization of a primary magma during magma re-injections or compositional convection (Hunter, 1987, 1996; Morse, 1988).

Temperature constraints from crystal habits

Because the crystallization of dendrites occurs under very specific thermodynamic conditions our interpretation of macrocrysts as dendrites has implications for their origin. In the experimental work of Faure *et al.* (2003*a*, 2007; Fig. 15), olivine develops a dendritic habit by rapid growth at a strong degree of undercooling ($-\Delta T > 60^{\circ}C$; i.e. the temperature drops below the liquidus) and for any cooling rate $\geq 47^{\circ}C\,h^{-1}$ within the magma. Conversely, crystals develop a skeletal habit at a moderate degree of undercooling ($-\Delta T = 20$–$60^{\circ}C$) and a polyhedral habit at a low degree of undercooling ($-\Delta T < 20^{\circ}C$). When the degree of undercooling increases well above 60°C, the morphology of olivine evolves rapidly from hollow (baby swallowtail habit: hopper with a few parallel replicas) to a true dendrite (swallowtail habit: hopper with numerous parallel, reduced-size replicas). In our samples, the occurrence of parallel groups varying from a few (Figs 5b, d, 6e, 7a–d, 8a, b, 9a–d and 10a–c) to tens of units (Figs 7e, 8c, d and 10d–f) may therefore result from morphological gradations throughout the dendritic growth of olivine in response to strong degrees of undercooling.

As shown by Fowler and co-workers (Shore & Fowler, 1999; Fowler *et al.*, 2002), olivine grows preferentially along its short *a*-axis because heat transfer is more efficient in this direction. Elongated olivine crystals (Figs 5c, d, 6d, e and 7c, d), such as spinifex olivine in komatiites, have been obtained experimentally by imposing a strong thermal gradient on an Mg-rich magma ($\sim 20^{\circ}C\,cm^{-1}$ and cooling rates at 2–5°C h^{-1}, Faure *et al.*, 2006). We therefore interpret the elongated units of macrocrysts as evidence that dendritic crystallization occurred in a thermal gradient. The fact that these elongated units have an unfaceted extremity (Fig. 7c and d) indicates that olivine grew on a substrate. Given the scarcity of these crystals, the thermal gradient is probably not strong ($< 20^{\circ}C\,cm^{-1}$) and/or is effective only within a small layer of the crystallizing magma. Similar olivine textures, called 'harrisites', have been shown to grow under such conditions in the layered series of the Rum Complex of Scotland (Harker, 1908; Wadsworth, 1961; Donaldson, 1974, 1976, 1977; O'Driscoll *et al.*, 2007).

Most olivine macrocrysts are composed of polyhedral units (Figs 5, 7c–e and 8–12) and only a few are skeletal (i.e. with hollow faces, Figs 6 and 7a, b). However, the initially skeletal habit of units is evidenced by the remaining cavities at the centre of polyhedral forms {021} (Fig. 7e, unit 1) and re-entrant P-rich zones (Fig. 12b). This suggests that each unit of the dendrite began with a skeletal habit, and then ripened towards a polyhedral habit by filling the hopper cavities into replete faces (i.e. reduction of the crystal surface). This indicates that the growth rate of olivine macrocrysts decreased during the course of crystallization (Fig. 16), which in turns implies that the initial disequilibrium of temperature and/or composition between olivine and its growth liquid has been reduced throughout crystallization. A first possibility is that the temperature of the magma increased at the contact with olivine. This may be due to a re-heating event by refilling of the reservoir and/or by transport of olivine crystals from cooler to hotter magmas. For example, Faure & Schiano (2005) have shown that an olivine dendrite formed far from equilibrium ($-\Delta T = 118^{\circ}C$, $1890^{\circ}C\,h^{-1}$) experiences textural ripening during an ensuing re-heating ($-\Delta T = 30^{\circ}C$ during 10 min). Welsch *et al.* (2009) have proposed that such thermal cycles can occur in a shallow magma reservoir through convection, with temperatures oscillating above the liquidus of clinopyroxene (1140°C) and below that of olivine (1230°C). Another possibility is that the degree of undercooling decreases by differentiation of the growth liquid. Indeed, crystallization is self-inhibited by the depletion of the liquid in olivine components (mainly MgO) and the decrease of the related liquidus temperature. For example, an undercooling of ~100°C in the binary system forsterite–fayalite can be neutralized by differentiation of the liquid from $Fo_{80}Fa_{20}$ to $Fo_{57}Fa_{43}$ (Fig. 17). The dendritic growth of olivine also involves a rapid depletion of olivine constituents (Si, Mg and Fe) in the interfacial liquid, yielding a boundary layer enriched in incompatible elements (P, Cr, Al,...); that is, a transient dead zone at the surface of the crystal (e.g. Cabrera & Vermilyea, 1958; Chernov, 1974; Sangwal, 1996). This poisoning of crystal faces may act as a chemical barrier between the mineral and its growth liquid, slowing down crystallization. This may explain the final polyhedral habit of each unit forming olivine macrocrysts. It is, however, unlikely that the crystallization of dendritic olivine rises to build up latent heat and force the growth rate to decrease because the diffusion of heat is several orders of magnitude faster than that of elements in the melt (Kirkpatrick, 1975, 1981). Depending on their crystallization history (i.e. the ratio dendritic growth/polyhedral growth) and considering an initial rapid growth rate at $10^{-6}\,m\,s^{-1}$ and a final slow rate at $10^{-9}\,m\,s^{-1}$ (Jambon *et al.*, 1992), it may be estimated that a typical olivine macrocryst (ø 0·5–5 mm) has crystallized in 8 min to 58 days.

Downloaded from http://petrology.oxfordjournals.org/ at University of Hawaii at Manoa Library on February 13, 2013

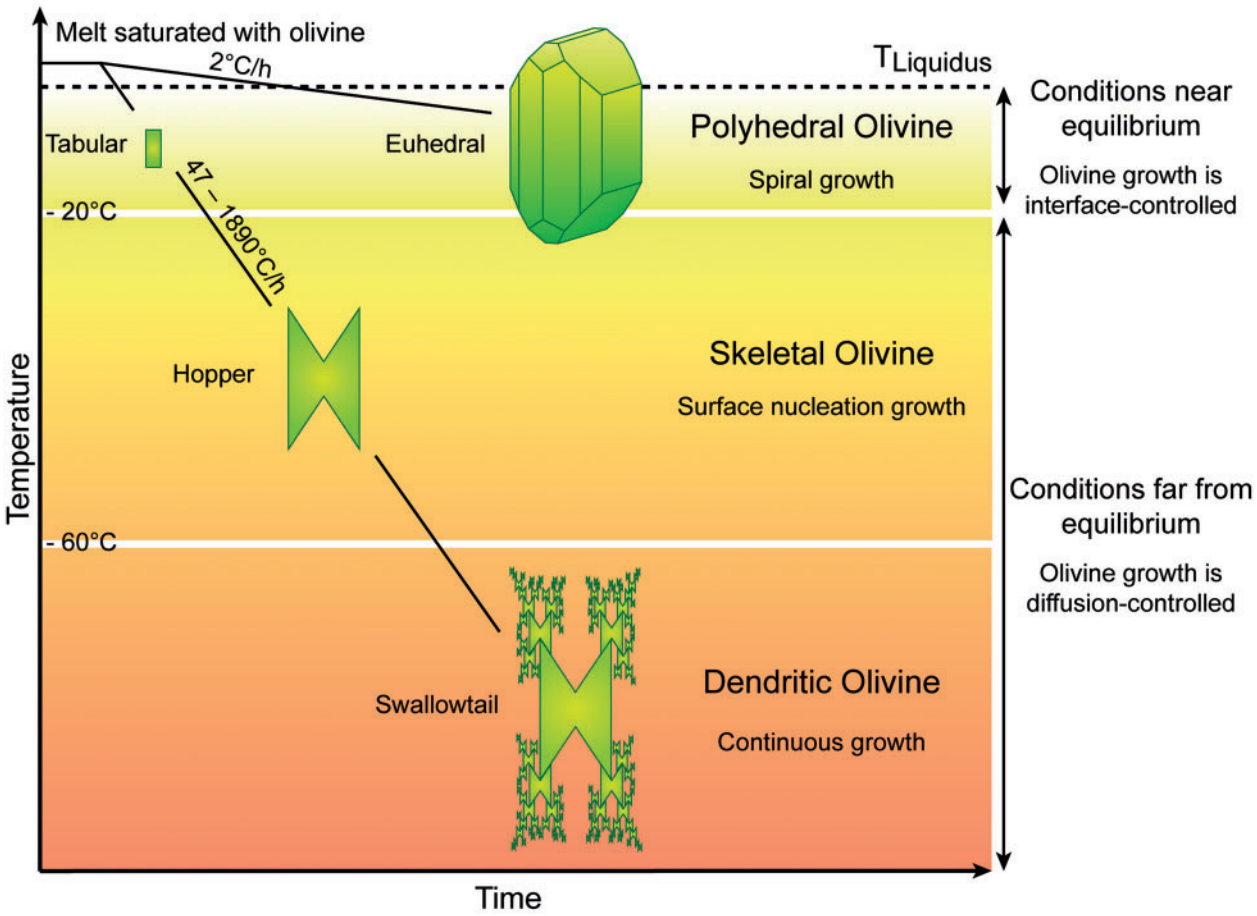

Fig. 15. Evolution of olivine habits as a function of the cooling rate and the nominal degree of undercooling ($-\Delta T = T_{liquidus} - T_{quench}$) determined in the CaO–MgO–Al_2O_3–SiO_2 system. Modified after Faure *et al.* (2003*a*, 2007). By increasing the degree of undercooling, the habit evolves following the sequence polyhedral > skeletal > dendritic, consistent with the classic models of Saratovkin (1959) and Sunagawa (1981). Polyhedral olivine (i.e. euhedral; see Fig. 2) crystallizes at low cooling rate (<47°C h^{-1}). In these conditions near equilibrium (Fowler & Roach, 1996), the liquid has a large period of time to re-equilibrate by crystallizing modest amounts of olivine. The transfers of constituents towards olivine are slight and the kinetics of crystallization is limited by the attachment rates of constituents at the surface of the crystal: the growth is interface-controlled [Burton–Cabrera–Frank mechanism (Burton *et al.*, 1951); i.e. spiral growth around dislocations involving a smooth surface and a low surface energy (Cabane *et al.*, 2005)]. Olivine consumes Mg, Fe and Si from the liquid at its contact and rejects the others elements. Because olivine grows slowly (~10^{-8} to 10^{-9} m s^{-1}; Jambon *et al.*, 1992), the liquid can re-homogenize with the far-field liquid by diffusion (provided that the viscosity of the melt remains low). Skeletal olivine (polyhedral habit with hollow faces) grows at moderate degrees of undercooling ($-\Delta T = 20$–60°C) and high cooling rates (47–1890°C h^{-1}). In these conditions, far from equilibrium, the liquid has a short time to crystallize a large amount of olivine. The kinetics of crystallization is limited by the diffusion rate of elements in the liquid: the growth is diffusion-controlled (surface nucleation involving surface roughening with higher surface energy; Faure *et al.*, 2007). Because olivine grows faster (~10^{-7} m s^{-1}; Jambon *et al.*, 1992) than the diffusion of some elements, the liquid in contact becomes depleted in elements compatible with olivine. Slow-diffusing impurities are accumulated at its contact and form a boundary layer, prohibiting growth at the centre of faces. Growth persists, however, at the edges and summits owing to the presence of larger volumes of liquid in these zones (Chernov, 1974), inducing the development of hollow faces: this is the 'Berg' effect (Berg, 1938). Dendritic olivine (branching habit) crystallizes at a strong degree of undercooling ($-\Delta T > 60$°C) and high cooling rates (47–1890°C h^{-1}). As for skeletal olivine, the growth process is diffusion-controlled (continuous growth mechanism; Faure *et al.*, 2007) but at higher rates (~10^{-6} m s^{-1}; Jambon *et al.*, 1992). Because the differentiation of the liquid involves a decrease of the liquidus temperature at the contact with olivine, growth is promoted for any protuberance at the surface of the crystal. By this effect of constitutional supercooling, the edges and summits develop skeletal extensions in the liquid, yielding a pseudo-fibre with a hierarchical pattern and swallowtail-type shape.

Geochemical implications of olivine growth mechanisms

Dendritic growth explains P-rich zones

The occurrence of P-rich zones in olivine macrocrysts (Fig. 12; Table 2) indicates that these crystals incorporated abnormal amounts of P during their crystallization. Given their sharp shapes and the low diffusion rate of P in olivine (Milman-Barris *et al.*, 2008), these P-rich zones probably experienced very little transport in the mineral, and probably retain their original position of formation.

Downloaded from http://petrology.oxfordjournals.org/ at University of Hawaii at Manoa Library on February 13, 2013

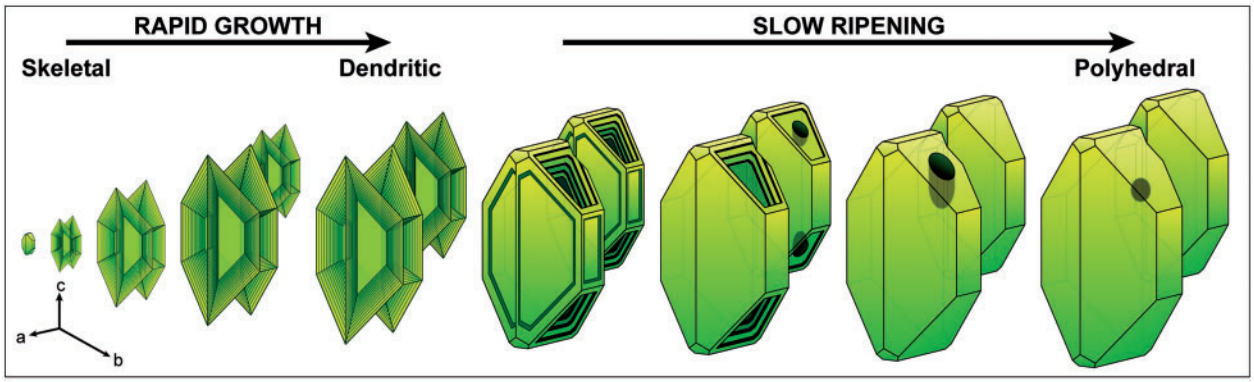

Fig. 16. Growth history of olivine macrocrysts. After nucleation, olivine crystallized rapidly from the liquid with a skeletal habit by developing hollow faces {021} and {001}, and possibly {110} with the privileged growth of edges and summits (i.e. the Berg effect). Olivine subsequently acquired a dendritic habit by rapid propagation of edges and summits within the liquid as new crystal replicas (effect of constitutional supercooling). With impurity poisoning and liquid differentiation, the mineral changed its growth mechanism and crystallized at a slower rate with a polyhedral habit. This step of olivine ripening involves the development of faces {001}, the infilling of hollow faces {021} and {110}, and the related formation of embayments and melt inclusions. Given the morphology of formerly hollow faces (Figs 6 and 7a, b and e), it is probable that olivine traps melt inclusions by overhanging new growth layers above its skeletal cavities. The occurrence of some remaining skelelal morphologies in olivine macrocrysts suggests that the infilling of hollow faces is a slow process that can be interrupted by the transport of crystals to the surface.

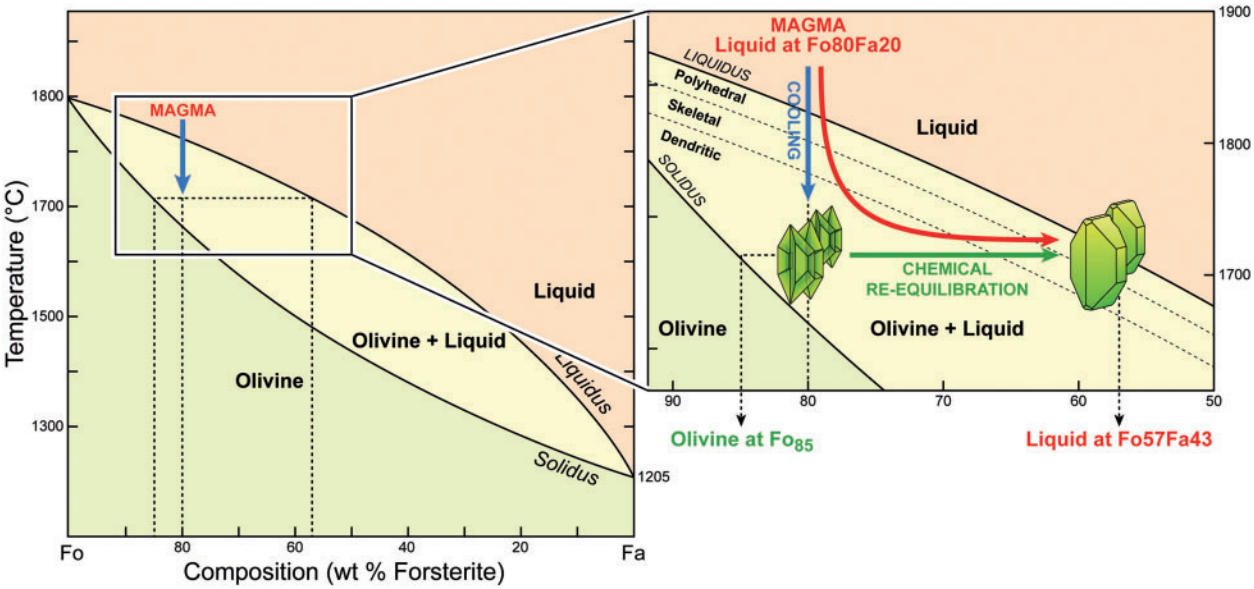

Fig. 17. Thermodynamic history of olivine macrocrysts in the Fo–Fa system (Bowen & Schairer, 1935) by crystallization of an MgO-rich magma with initial composition at $Fo_{80}Fa_{20}$. An initial undercooling ($-\Delta T$) of 100°C below the olivine liquidus causes the dendritic crystallization of Fo_{85} olivine. The chemical re-equilibration of the system implies the differentiation of the liquid from $Fo_{80}Fa_{20}$ to $Fo_{57}Fa_{43}$ and the polyhedral ripening of dendritic olivine in conditions approaching equilibrium.

To understand how such zoning forms, it is important first to determine the shape and the number of these zones in the olivine macrocrysts. All the zoning patterns depict a single, P-rich skeletal core at the centre of each crystal unit, with re-entrant shapes outlining ancient hopper cavities (Fig. 18). This explains why sections perpendicular to these hopper cavities show concentric P-rich benches separated by P-poor gaps, leading to oscillatory zoning similar to that shown in Fig. 12a. Conversely, oblique sections through the P-rich skeletal core and P-poor ripened zones expose the ancient walls of hopper cavities, yielding a 'herring-bone' pattern of interconnected P-rich benches (figs 1a, e, 2a and 3e, f of Milman-Barris *et al.*, 2008). We emphasize that all the P-rich zones of a given unit must be connected in three dimensions. Because each crystal unit results from the splitting growth of a unique lattice, it is probable that the P-rich zones are also interconnected from one crystal unit to another within a single group

Downloaded from http://petrology.oxfordjournals.org/ at University of Hawaii at Manoa Library on February 13, 2013

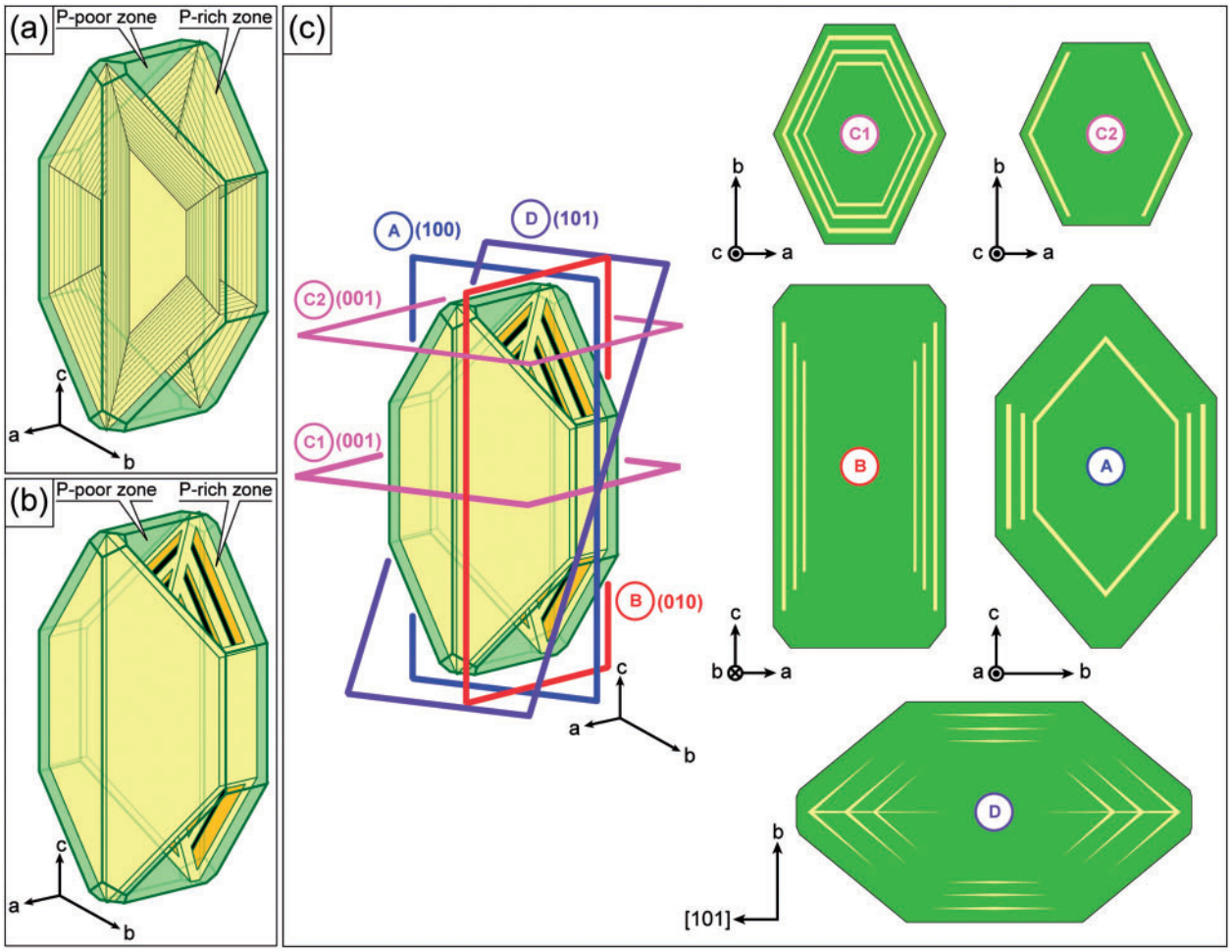

Fig. 18. Interpretative sketch of P-rich zoning occurring within each crystal unit of olivine macrocrysts. Light, P-rich zones; dark, P-poor zones. The true shape of the P-rich zones may vary from (a) entirely skeletal (all the faces are hollow with many terraces) to (b) partially skeletal (the model is based on the crystal of Fig. 7a, considering hollow forms {021} and {001} with, at the centre of the crystal, three concentric terraces interconnected by their edges). (c) Zoning patterns obtained by sectioning model (b). Section A—plane (100): hexagonal zoning similar to fig. 5g–i of Milman-Barris *et al.* (2008). Section B—plane (010): zonings parallel to forms {010} similar to fig. 2c of Milman-Barris *et al.* (2008). Section C1—plane (001): concentric zoning by intersecting the three terraces occurring at the core (similar to Fig. 12a; also fig. 4 of Milman-Barris *et al.*, 2008). Section C2—plane (001): simple zoning by intersecting only one terrace in the vicinity of the rim (similar to Fig. 12c; also figs 1c, 2b and d of Milman-Barris *et al.*, 2008). Section D—plane (101): herring-bone or feathery zoning of the literature (figs 1a, e, 2a and 3e–f of Milman-Barris *et al.*, 2008). The connections between the terraces correspond to the older summits and edges of the crystal unit formed during constitutional supercooling. It should be noted that these P-rich edges can be exposed with other oblique sections.

(these interconnections are probably not observed in element maps because they are rarely intersected by sections; e.g. Dowty 1980*b*). If so, each group of parallel units is built on a fibrous network of interconnected hopper units enriched in P. This reconstruction has two implications: first, these zones have recorded only one main event of crystallization; second, this event occurred during the dendritic growth of olivine. The only exception is the P-rich zone located at the contact with the mesostasis, which probably results from melt solidification at the crystal surface.

Milman-Barris *et al.* (2008) obtained olivine crystals with similar P-rich zones in experiments of simple cooling within P_2O_5-bearing melts, showing that these zones are due to processes intrinsic to olivine growth from the liquid, rather than to external processes such as magma convection or mixing. Importantly, those workers also noticed that the liquid in contact with the growing olivine was enriched with P_2O_5 (by ~20 wt %). Because the matrix glasses of the Piton de la Fournaise lavas contain 0·3–0·6 wt % P_2O_5 (Table 2) and given the low diffusion rates of P in silicate liquids (Harrison & Watson, 1984), it is likely that this element accumulated at the contact with the olivine macrocrysts during their rapid dendritic growth. Olivine formed zones from this boundary layer enriched in P_2O_5 only during its dendritic growth and not

Downloaded from http://petrology.oxfordjournals.org/ at University of Hawaii at Manoa Library on February 13, 2013

after, because the external parts of its dendritic habit are depleted in this element (Fig. 12). It is beyond the scope of this study to determine which process amongst adsorption, elastic partitioning, pinning of elementary step or macrostep motion, impurity uptake or solute trapping drives the incorporation of P, Al and Cr (e.g. Dowty, 1977; Blundy & Wood, 1994; Sangwal, 1996; Land *et al.*, 1999).

Dendritic growth and ripening explain Cr-spinel and melt inclusions

The crystallization of Cr-spinel is intimately linked with olivine crystallization as this phase is frequently associated with olivine (Figs 7–11), and rarely occurs alone in the matrix glasses or in association with other minerals (such as groundmass clinopyroxene or plagioclase, Welsch *et al.*, 2009). Its frequent occurrence within olivine-hosted melt inclusions could suggest that Cr-spinel is a daughter mineral crystallized from these pockets of liquid after their entrapment in olivine. This is, however, unlikely because the high Cr_2O_3 contents of spinel (30·98–41·21 wt %; Table 2) would imply an unrealistic Cr concentration in the trapped liquid (Clocchiatti *et al.*, 1979), provided that Cr_2O_3 is a minor oxide in the matrix glasses (<0·15 wt %) and primary magmas (~0·3 wt %, Famin *et al.*, 2009). On the other hand, the crystallization of Cr-spinel may result from the accumulation of Cr in the boundary layer of dendritic growing olivine (e.g. Maaløe & Hansen, 1982; Bacon, 1989), as Cr_2O_3 is a trace oxide in olivine (<0·10 wt %, Table 2) and a major oxide in spinel. In this case, the systematic cluster occurrence of Cr-spinel with olivine may indicate that Cr-spinel crystallized *in situ* reflecting local supersaturation (Fig. 19).

The occurrence of Cr-spinel microcrysts in olivine-hosted melt inclusions and embayments could also suggest that olivine sealed portions of its own boundary layers (Faure & Schiano, 2005). This assertion may, however, be discarded because these melt inclusions do not show significant enrichment in slow-diffusing impurities such as Al, Ca and P relative to the matrix glass (Table 2; Harrison & Watson, 1984; Liang *et al.*, 1996). Small and large melt inclusions have similar compositions, without applying any correction for post-entrapment processes (Famin *et al.*, 2009; see also Table 2). This indicates that these melt inclusions were re-homogenized with the far-field liquid (by diffusion and/or convection) before their complete sealing in olivine (e.g. Kohut & Nielsen, 2004). If so, these melt inclusions were encapsulated during the slow ripening of olivine and not during its rapid, dendritic growth (Fig. 19). This suggests that these melt inclusions preserve genetic relationships with their host olivine and the matrix glasses of the basalts, allowing the reconstruction of the liquid-line of descent of the Piton de la Fournaise parental magmas (Clocchiatti *et al.*, 1979; Famin *et al.*, 2009).

Possible origins of xenocrystic textures

Many olivine macrocrysts from Piton de la Fournaise and Hawaii have been classified as xenocrysts on the basis of textural criteria (deformation [i], dissolution [iii] and fractures [iv] of Helz, 1987) and chemical criteria of disequilibrium (Albarède & Tamagnan, 1988; Albarède *et al.*, 1997). However, our recognition of the dendritic growth mechanism of olivine macrocrysts brings an alternative interpretation to the origin of these textures and chemical disequilibrium, as summarized in Table 4.

Plastically deformed crystals [i]

Olivine macrocrysts with planar defects such as subgrain boundaries or dislocation lamellae (Fig. 10b–f) have been interpreted as plastically deformed crystals extracted from a tectonized dunite (Helz, 1987; Albarède & Tamagnan, 1988; Clague & Denlinger, 1994; Albarède *et al.*, 1997; Vinet & Higgins, 2010; Vinet *et al.*, 2011). This interpretation is, however, in contradiction to the external, undamaged growth faces exhibited by olivine macrocrysts (Figs 5–12), which indicate that these crystals grew in suspension within the magma. The fact that their P-rich zonings are parallel to these growth faces (Fig. 12) indicates that olivine rims did not come into contact with other solids, or experience significant amounts of resorption into the magma. This invalidates the assumption that olivine macrocrysts are 'euhedral xenocrysts'; that is, dunite grains that have developed growth forms after incorporation into the magma (e.g. Boudier, 1991). Olivine macrocrysts may have been deformed in the melt by collision (e.g. Natland, 2003) during their transport [although there is no evidence of impacts at their surface (Figs 5–8) or indentation of their chemical zones (Fig. 12)] or by viscous flow (e.g. Deubelbeiss *et al.*, 2011). Alternatively, Sunagawa (2005) suggested that lattice mismatches (i.e. point and planar defects) may occur where the side branches of a dendritic crystal merge, when an inclusion is enclosed during growth, or at the boundary of two slightly misoriented crystals. Our study shows that olivine macrocrysts have such dendritic growth, Cr-spinel and melt inclusions (Fig. 11), and slight misorientations of their crystal units (Figs 7a, b, 8a and 10b–d). Hence, some crystal defects formerly interpreted as the result of intracrystalline deformation may in fact be the consequence of olivine crystallization in a melt. For instance, planar defects in olivine interpreted as subgrain boundaries in response to grain boundary migration recrystallization (e.g. Passchier & Trouw, 1998) probably result from the contact between growing units with an imperfect alignment in a mosaic macrocryst (referred to as 'lineage structure' by Buerger, 1932, 1934; Drever & Johnston, 1957; Figs 8c, d and 10b–d). Faure *et al.* (2003*b*) experimentally obtained planar defects in olivine dendrites grown in conditions very far from equilibrium ($-\Delta T = 300^\circ C$, $1890^\circ C\,h^{-1}$), without any

Downloaded from http://petrology.oxfordjournals.org/ at University of Hawaii at Manoa Library on February 13, 2013

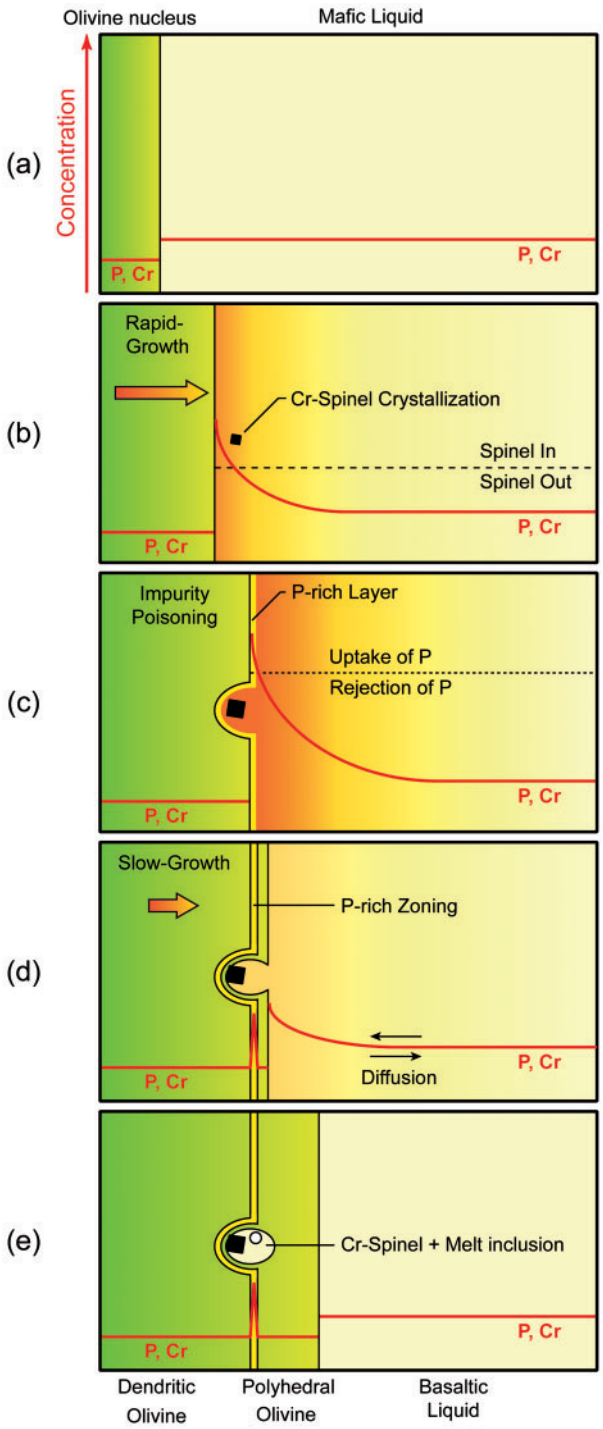

Fig. 19. Interpretative sketch for the formation of P-rich zonings, Cr-spinel and related melt inclusions within olivine from a liquid initially depleted in P and Cr. (a) Before dendritic growth, each olivine nucleus may have grown slowly from the liquid without having accumulated slow-diffusing, incompatible elements (P, Cr) in the liquid at its contact (conditions near equilibrium). (b) Because of the strong undercooling, olivine started to grow rapidly with a dendritic habit in the liquid, leading to the accumulation of P and Cr at its contact (conditions far from equilibrium). The local increase of Cr in the liquid promoted the crystallization of Cr-spinel at the contact with dendritic olivine. (c) The rapid growth of olivine and the continuing accumulation of P in the boundary layer led to incorporation of higher P contents in the lattice, yielding a thin layer of olivine enriched in P. (d, e) With continuing crystallization and differentiation of the liquid, the olivine growth rates decreased, inducing a polyhedral growth. This ripening progressively buried the layer enriched in P as zonings (fossilizing its original dendritic habit), and embayed and trapped the Cr-spinel crystals nucleated at the contact with olivine as solid inclusions with or without melt around them. The scale in the sketch is arbitrary.

deformation. Similarly, dislocation lamellae interpreted as deformation bands may also result from the migration and concentration of point and linear defects in the weakness planes of olivine (Fig. 10e and f; Poirier, 1975), such as cleavage planes (100), (010) and (001). In a similar way, textures of slight and discontinuous undulose extinction such as in Fig. 10b and e could also be attributed to slight misalignments between units and/or to the migration of defects stopped before the formation of true dislocation lamellae.

Corroded crystals [iii]

Crystals with rounded outlines have previously been interpreted as evidence of resorption (or corrosion) by thermal and/or chemical disequilibrium with the fluid with which they are in contact (e.g. Helz, 1987; Albarède & Tamagnan, 1988). However, this fluid does not need to be genetically unrelated to the macrocrysts to yield corroded textures. Indeed, Drever & Johnston (1957) suggested that olivine reacts with the residual liquid after differentiation by crystallization of clinopyroxene, plagioclase and Fe–Ti-oxides. This is confirmed by the fact that olivine has sharp edges in lapilli and glass-rich mesostasis (Figs 5–8, 9c–f, 10a–d and f) and rounded edges in glass-poor, crystallized mesostasis (Figs 9a, b and 10e). Consequently, the rounded texture of macrocrysts may result from subsurface cooling or sampling and does not necessarily reflect a xenocrystic origin. Similarly, embayments in olivine, formerly interpreted as local dissolution (e.g. Roedder, 1979) are not evidence of a xenocrystic origin, because they are due to a local lack of growth. This lack of growth may be due to the formation of a melt inclusion by anchoring of screw-dislocations during polyhedral growth (Faure & Schiano, 2005), or to Cr-spinel microcrysts in contact with the olivine (Fig. 19). In the latter case the Cr-spinel microcrysts may not be apparent in thin section depending on its orientation.

Fractured crystals [iv]

Crystals displaying cleavage surfaces, conchoidal fractures or shapes in disagreement with the growth habit of olivine have been interpreted as fragments resulting from magmatic deformation; for instance, by collision with nearby crystals or the walls of the magma system on their way to

Downloaded from http://petrology.oxfordjournals.org/ at University of Hawaii at Manoa Library on February 13, 2013

Table 4: Major characteristics of olivine macrocrysts and interpretations (see text for details)

Features of olivine macrocrysts	Previous interpretations	Alternative interpretations
Their cores are in disequilibrium with the glassy matrix ($K_{D\ Fe\text{-}Mg} \neq 0{\cdot}3 \pm 0{\cdot}03$)	Olivine is genetically unrelated to its host liquid [1, 2]	Olivine is in contact with the differentiated part of its parental liquid
Their cores have a homogeneous Fe–Mg composition	Fe^{2+} and Mg^{2+} interdiffused at magmatic temperatures	Fe^{2+} and Mg^{2+} interdiffused at magmatic temperatures
Each macrocryst is composed of several crystal units	Each macrocryst is the result of the attachment of smaller crystals [3]	Each unit is a bud of a single dendritic crystal
Crystal units have parallel orientations	The units are separated crystals attached by their parallel faces [3]	The units result from the splitting growth of a single lattice
Crystal units show a hierarchy in the grouping	—	The dendrite propagated as a chain of smaller crystal units (constitutional supercooling)
Crystal units are elongated along the *a*-axis	—	The units grew along a thermal gradient (constrained growth)
Each group of units has a shape similar to a single olivine crystal	—	The original habit of olivine is preserved by the dendrite (mosaic structure)
Subgrain boundaries	The crystals deformed plastically when they were forming a compacted cumulate [1, 4]	The dendrite formed planes of dislocations at the junctions of growing misaligned units (lineage structure)
Dislocation lamellae	The lattice defects have migrated in the planes of weakness at magmatic temperatures [5]	The lattice defects have migrated in the planes of weakness at magmatic temperatures [5]
Undulose extinction	The crystals were deformed plastically when they were forming a compacted cumulate [1, 4]	Faint dislocation lamellae
Crystal units are well-faceted (in glassy mesostasis)	Olivine dissolved at low rates or recrystallized after extraction from the cumulate [6]	Olivine crystallized from the magma (dendritic growth then ripening)
Crystal units are rounded (in crystallized mesostasis)	Olivine dissolved during its extraction from the cumulate and/or during its transport to the surface [4]	Olivine reacted with the residual liquid during the slow solidification of lava flows [7]
Melt inclusions	Olivine trapped magmas during growth and/or during healing of fractures [8]	Olivine sealed off the cavities formed by dendritic growth during final ripening
Sulfide inclusions	Olivine crystallized from deeper magmas enriched in S [4, 9]	The S composition of the parental magma is heterogeneous because of immiscibility
Cr-spinel inclusions	Olivine trapped Cr-spinel crystallized from primitive magmas? [10]	The impurities rejected by the dendritic growth of olivine promoted a local supersaturation with Cr-spinel [11]

[1] Albarède & Tamagnan (1988); [2] Albarède *et al.* (1997); [3] Schwindinger & Anderson (1989); [4] Helz (1987); [5] Poirier (1975); [6] Boudier (1991); [7] Drever & Johnston (1957); [8] Bureau *et al.* (1998*a*); [9] Bureau *et al.* (1999); [10] Roeder *et al.* (2006); [11] Maaløe & Hansen (1982).

Downloaded from http://petrology.oxfordjournals.org/ at University of Hawaii at Manoa Library on February 13, 2013

the surface (e.g. Natland, 2003). However, sectioning effects may produce many of the fractured shapes observed in thin section. For instance, an euhedral crystal can display a triangular shape if cut at an oblique angle to all the faces, yielding a type [iv] crystal (Supplementary Data, Appendix 1). Olivine may also be fragmented during sectioning, or scratched during polishing, yielding irregular cavities devoid of glass and minerals in the grain's interior and/or at the contact with the mesostasis. Conchoidal fractures and cleavage surfaces may be due to thermal cracking of the olivine crystals (especially those containing Cr-spinel microcrysts, Figs 8d and 11b) during their ascent to the surface (e.g. Albarède & Tamagnan, 1988). It is therefore difficult to conclude that fractured crystals originated from magmatic deformation rather than from their ascent to the surface or from preparation artefacts.

Euhedral crystals with sulfide inclusions [v]

Sulfide inclusions are inferred to result from olivine crystallization in a magma enriched in S (Helz, 1987), distinct from the parental magma of other olivine classes. However, because S-saturated melts are immiscible (Haughton *et al.*, 1974; O'Neill & Mavrogenes, 2002), the sulfide concentration of the magmatic reservoir is probably highly heterogeneous and may depend on density contrasts. As a consequence, olivine growth may occur with or without sulfide inclusions, depending on their location in a single reservoir. In this case, the existence of a separate S-enriched magma may be hardly evidenced from the entrapment of an immiscible liquid.

Chemical disequilibrium

Some olivine macrocrysts have been classified as xenocrysts because their homogeneous (i.e. unzoned) Fe–Mg contents are in disequilibrium with the host liquid (e.g. Albarède & Tamagnan, 1988; Albarède *et al.*, 1997). However, two mechanisms may disturb the chemical equilibrium between an olivine crystal and its growth liquid without a xenocrystic origin. (1) Because fast skeletal and dendritic growths are diffusion-controlled (Faure *et al.*, 2003*a*, 2007; Fig. 15), the composition of the liquid in contact with the crystal is depleted in Mg and enriched in incompatible elements, yielding Fo-depleted olivine with respect to the far-field liquid (see also Maaloe, 2011, for implications). (2) Fast Fe–Mg interdiffusion in olivine at magmatic temperatures is prone to erase any Fe–Mg zoning acquired during partial crystallization, yielding homogeneous crystals that are not in equilibrium with either the initial liquid or the residual liquid. As a consequence, it is difficult to conclude that olivine macrocrysts are xenocrysts based on chemical Fe–Mg disequilibrium with the host liquid.

A unifying concept for olivine textures

A major consequence of our study is that six ([i]–[v] and [vii]) of the seven crystal classes defined by Helz (1987) may all be derived from type [ii] euhedral and skeletal crystals. For instance, blocky, irregular crystals [i] may be interpreted as euhedral crystals [iia], with an extreme density of parallel units and the presence of dislocation lamellae (Fig. 10e and f). Megacrysts [vii] are similar to blocky, irregular crystals [i], but they are formed with more or larger crystal units (e.g. large crystal in Fig. 3j). Rounded [iii] and angular crystals [iv] are also built up with euhedral parallel units of type [ii] (Figs 9a, b and 10e). Euhedral crystals with sulfide inclusions [v] may belong to type [iia], as may euhedral crystals containing Cr-spinel or melt inclusions. These variants of type [ii] are due to variations of habit, size and density of crystal units, and defects and inclusions in macrocrysts, which may all result from the dendritic growth and subsequent ripening of olivine.

It could be possible to separate type [vi] olivine aggregates (Helz, 1987; Supplementary Data, Appendix 1) found in dunite enclaves and mesocryst clusters from the six other macrocryst types because of their non-ordered crystal pattern (Figs 13 and 14). In the case of Piton de la Fournaise, however, there is ample evidence that olivine aggregates are cumulates of macrocrysts, as follows. (1) Olivine aggregates occur together with olivine macrocrysts in the same lavas (Fig. 3j, see also Welsch *et al.*, 2009). (2) Mosaic macrocrysts and crystals containing Cr-spinel, melt and sulfide inclusions are all found in dunite enclaves (Fig. 14c–f). (3) Dunites contain crystals with subgrain boundaries and dislocation lamellae in contact with crystal without defects (Fig. 14c and d), suggesting that these defects have been acquired before the aggregation. (4) Crystal aggregates and macrocrysts have close compositional ranges (Table 2; see also Upton *et al.*, 2000; Famin *et al.*, 2009; Welsch *et al.*, 2009). This indicates that dunite enclaves are not mantle xenoliths, but fragments of cumulates. In consequence, we propose that all the textures of olivine may derive from type [ii]; that is, dendritic growth and ripening.

Implications for magma chamber dynamics

Our study of olivine-rich basalts from Piton de la Fournaise suggests that olivine macrocrysts have a unique origin: an early rapid dendritic growth owing to strong undercooling. Experimental results indicate that the dendritic growth of olivine requires a minimal undercooling of 60°C within the melt (Faure *et al.*, 2003*a*), which is in good agreement with a temperature difference of 50–90°C between the liquidus of Fo_{84} olivine (1220–1240°C; Welsch *et al.*, 2009) and the temperature of magmas erupted at the surface (1150–1170°C; Coppola *et al.*, 2007; Boivin & Bachèlery,

Downloaded from http://petrology.oxfordjournals.org/ at University of Hawaii at Manoa Library on February 13, 2013

2009). This strong undercooling may not be explained by loss of volatiles because (1) harrisitic olivine crystallizes both in water-saturated and under-saturated conditions (Donaldson, 1977), (2) primary, hydrous minerals occur in harrisitic cumulates (Donaldson, 1982), and (3) degassing has little effect on the liquidus of olivine (variations <20°C in Piton de la Fournaise magmas; Welsch *et al.*, 2009). We speculate that the strongest temperature gradients, and hence the strongest undercooling, occur at the walls of the shallow reservoir after each new arrival of hot and MgO-rich magma (e.g. Jaupart *et al.*, 1984; Marsh, 1989). Five of such replenishment episodes have been evidenced at Piton de la Fournaise between 1998 and 2007 (see Coppola *et al.*, 2009, and references therein). The temperature difference between the hot magma (≥1170°C) and the country rock (646°C for the glass transition in Piton de la Fournaise basalts; Villeneuve *et al.*, 2008) is so large that dendritic olivine grows on or near the walls of the reservoir, forming a rim of mush (Fig. 20). A similar process has been proposed to explain the dendritic textures

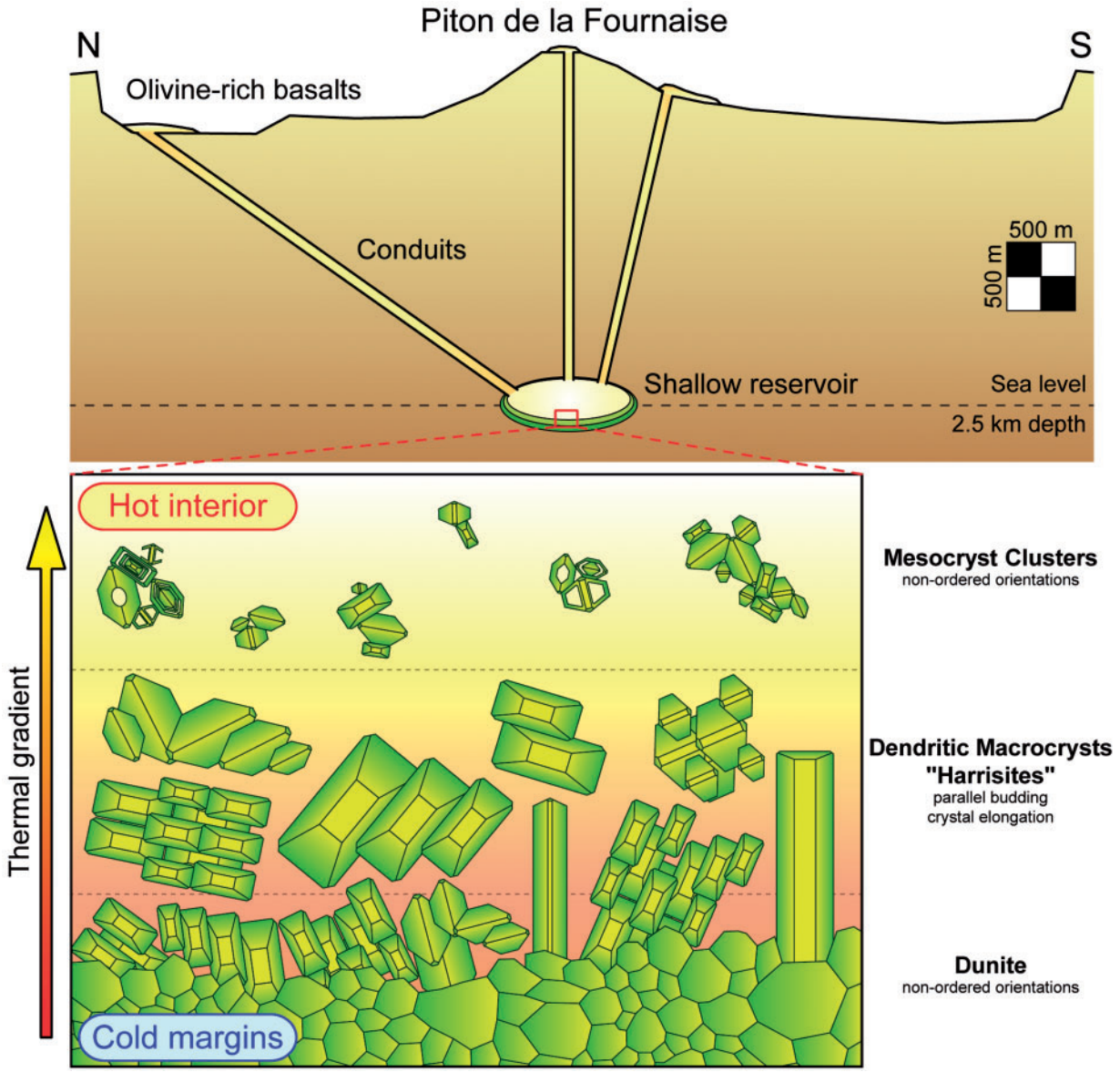

Fig. 20. Interpretative sketch of the harrisitic mush yielding the magnesian basalts, picrites and oceanites erupted at Piton de la Fournaise volcano (arbitrary scale). Olivine macro- and mesocrysts result from the progressive crystallization of an MgO-rich magma within the weak thermal gradient developed near the cold margins of the shallow reservoir. The textures and layering within the mush are similar to the harrisites described in the Rum Complex (Donaldson, 1977). Upon aggregation, settling and adcumulus processes (e.g. Wager *et al.*, 1960; Hunter, 1987, 1996; Morse, 1988), olivine macro- and mesocrysts may intergrow and form a compacted layer resistant to magmatic withdrawal. In rare cases of strong magma turbulence, this dunitic layer may be fragmented and transported at the surface as enclaves embedded within the magma.

Downloaded from http://petrology.oxfordjournals.org/ at University of Hawaii at Manoa Library on February 13, 2013

identified in the layered series of many frozen magma chambers (Harker, 1908; Wager & Brown, 1951, 1968; Taubeneck & Poldervaart, 1960; Wager *et al.*, 1960; Moore & Lockwood, 1973; Ohnenstetter *et al.*, 1975; Wilkinson *et al.*, 1975; Petersen, 1978, 1985; Thériault & Fowler, 1995).

After rapid dendritic growth, the macrocrysts ripened slowly towards a polyhedral habit. A necessary condition for this is the absence of strong cooling and heating cycles, because large temperature fluctuations (e.g. cooling at $-\Delta T > 70^{\circ}$C, with a rate $>437^{\circ}$C h^{-1} then re-heating at $-\Delta T > 34^{\circ}$C for 5 min) are known to yield typical crystal habits (closed hopper and complex swallowtail; Faure & Schiano, 2004; Welsch *et al.*, 2009) that are not observed in our olivine macrocrysts. The most favourable environment for the crystallization of olivine macrocrysts is therefore a low temperature gradient in a stagnant magma (i.e. no convection) undergoing differentiation (Figs 16 and 17). Because the magma is turbulent during eruptions (Welsch *et al.*, 2009), it is probable that the crystallization of olivine macrocrysts occurs only during the inter-eruptive periods. This is consistent with the fact that these crystals developed most of their growth shapes prior to the vesiculation of the magma (Fig. 5f).

The textural difference between a mush and a cumulate is probably an important rheological factor controlling the incorporation of olivine crystals in the magma. Because the rim of mush is unconsolidated at the margins of the shallow reservoir, it may be easily transported to the surface during eruptions, yielding extremely olivine-rich basalts (i.e. oceanites). On the other hand, olivine meso- and macrocrysts may form a compacted and more resistant layer once aggregated into a dunite (Fig. 14), making them less subject to magmatic remobilization and withdrawal. This rheological difference may have introduced a bias of transport, explaining the overwhelming occurrence of oceanites compared with dunite enclaves, despite a common origin.

Dendritic olivine occurs in many other porphyritic lavas over different geodynamic settings, including ocean island basalts (OIB), mid-ocean ridge basalts (MORB) and island arc basalts [IAB; see the reviews by Drever & Johnston (1957) and Milman-Barris *et al.* (2008)]. Porphyritic olivine basalts would thus be evidence that mantle-derived magmas are strongly undercooled within the crust (e.g. Maaløe, 2011). However, in other lavas, such as komatiites, kimberlites or ultramafic lamprophyres, the model may not apply, as these rocks have other olivine textures and compositions, and a different magma history (Pyke *et al.*, 1973; Kerr & Arndt, 2001; Brett *et al.*, 2009; Arndt *et al.*, 2010).

Implications for the interpretation of deformed olivine

Many textures of olivine (such as subgrain boundaries, dislocation lamellae and undulose extinction) have been formerly interpreted as caused by plastic intracrystalline deformation. In turn, this plastic deformation has been taken as evidence of a dunite body accommodating the spreading of Hawaiian volcanoes by deforming the olivine grains (Borgia, 1994; Clague & Denlinger, 1994). Based on the presence of these textures, the path of Kilauean olivine-rich magmas has also been inferred to go through the deforming dunite body (Helz, 1987; Clague & Denlinger, 1994; Vinet & Higgins, 2010). Creeping dunites have also been proposed to accommodate the deformation of Piton de la Fournaise volcano (e.g. Upton *et al.*, 2000). Some textures, such as undulose extinction, may indeed come from true deformation. However, our study shows that the majority of olivine textures may be produced by dendritic growth rather than by deformation. In consequence, we suggest that the importance of deformation in olivine, and its role in the slumping and spreading of basaltic volcanoes, may have been considerably overestimated.

CONCLUSIONS

Our study of the texture and composition of olivine macrocrysts from Piton de la Fournaise reveals that crystallization proceeds by a single mechanism of dendritic growth within the magma. This crystallization process provides an integrated explanation to a large number of textures observed in olivine, such as hollow faces, P-rich zoning, and melt and Cr-spinel inclusion entrapment, that have been previously interpreted as a combination of multiple mechanisms. Subgrain boundaries, dislocation lamellae and to a certain extent undulose extinction may also result from lattice mismatches caused by dendritic growth, and not only from plastic intracrystalline deformation. We suggest that all olivine macrocrysts are budding phenocrysts grown at a strong degree of undercooling, with a variable abundance of twins, inclusions and lattice mismatches depending on the conditions of temperature and composition. Olivine macrocrysts have grown in suspension within the liquid, and were neither aggregated into a dense cumulate nor corroded, shocked or deformed before or during their transport to the surface. The olivine-rich basalts of Piton de la Fournaise are therefore interpreted as a harrisitic mush crystallized on the cold margins of the shallow reservoir, and transported to the surface. Dunite cumulates result from the later aggregation and compaction of this mush. The first implication of our study is that the majority of olivine macrocrysts are not xenocrysts. The second implication is that the deformation of olivine cumulates, proposed to accommodate volcano spreading, may have been considerably overestimated.

ACKNOWLEDGEMENTS

We benefited from the helpful comments of Lotte Larsen, Nicholas Arndt and an anonymous reviewer on an early version of the paper. OVPF staff, Alain Barrère and

Downloaded from http://petrology.oxfordjournals.org/ at University of Hawaii at Manoa Library on February 13, 2013

Guillaume Falco collected some of the lava samples erupted in the period 2002–2007. Geneviève Lebeau, Cédric Demeurie and Jean-Luc Lemineur performed thin section preparation. We are also grateful to Sandrine Mathieu and Frédérick Couffignal for assistance with chemical mapping by electronic microprobe. We also benefited from discussions with Philippe Mairine, Khalid Addi, Brian Upton, Julia Hammer, Michael Garcia, Eric Hellebrand and Nicolas Vinet.

FUNDING

This work was sponsored by Fonds Social Européen, Région Réunion and Agence Nationale de la Recherche through grants ANR-06-CATT-013-01-VOLCARISK and ANR-07-BLAN-0130-CSD6-MIME. This is IPG Contribution No. 3319, CRPG No. 2195 and Laboratory of Excellence ClerVolc No. 43.

SUPPLEMENTARY DATA

Supplementary data for this paper are available at *Journal of Petrology* online.

REFERENCES

Aki, K. & Ferrazzini, V. (2000). Seismic monitoring and modelling of an active volcano for prediction. *Journal of Geophysical Research* **105**, 16617–16640.

Albarède, F. & Tamagnan, V. (1988). Modelling the recent geochemical evolution of the Piton de la Fournaise volcano, Réunion Island, 1931–1986. *Journal of Petrology* **29**, 997–1030.

Albarède, F., Luais, B., Fitton, G., Semet, M., Kaminski, E., Upton, B. G., Bachèlery, P. & Cheminée, J.-L. (1997). The geochemical regimes of Piton de la Fournaise volcano (Réunion) during the last 530–000 years. *Journal of Petrology* **38**, 171–201.

Amma-Miyasaka, M. & Nakagawa, M. (2002). Origin of anorthite and olivine megacrysts in island-arc tholeiites: Petrological study of 1940 and 1962 ejecta from Miyake-Jima volcano, Izu–Mariana arc. *Journal of Volcanology and Geothermal Research* **117**, 263–283.

Arndt, N., Lehnert, K. & Vasil'ev, Y. (1995). Meimechites: Highly magnesian lithosphere-contaminated alkaline magmas from deep subcontinental mantle. *Lithos* **34**, 41–59.

Arndt, N. T., Guitreau, M., Boullier, A. M., Le Roex, A., Tommasi, A., Cordier, P. & Sobolev, A. (2010). Olivine, and the origin of kimberlite. *Journal of Petrology* **51**, 573–602.

Bacon, C. R. (1989). Crystallization of accessory phases in magmas by local saturation adjacent to phenocrysts. *Geochimica et Cosmochimica Acta* **53**, 1055–1066.

Berg, W. F. (1938). Crystal growth from solutions. *Proceedings of the Royal Society of London, Series A, Mathematical and Physical Sciences* **164**, 79–95.

Blundy, J. & Wood, B. (1994). Prediction of crystal–melt partition coefficients from elastic moduli. *Nature* **372**, 452–454.

Boivin, P. & Bachèlery, P. (2009). Petrology of 1977 to 1998 eruptions of Piton de la Fournaise, La Réunion Island. *Journal of Volcanology and Geothermal Research* **184**, 109–125.

Borgia, A. (1994). Dynamic basis of volcanic spreading. *Journal of Geophysical Research* **99**, 17791–17804.

Boudier, F. (1991). Olivine xenocrysts in picritic magmas. *Contributions to Mineralogy and Petrology* **109**, 114–123.

Bowen, N. L. & Schairer, J. F. (1935). The system MgO–FeO–SiO_2. *American Journal of Science* **29**, 151–217.

Brett, R. C., Russell, J. K. & Moss, S. (2009). Origin of olivine in kimberlite: Phenocryst or impostor? *Lithos* **112** (Supplement 1): 201–212.

Buening, D. K. & Buseck, P. R. (1973). Fe–Mg lattice diffusion in olivine. *Journal of Geophysical Research* **78**, 6852–6862.

Buerger, M. J. (1932). The significance of block structure in crystals. *American Mineralogist* **17**, 177–191.

Buerger, M. J. (1934). The lineage structure of crystals. *Zeitschrift für Kristallographie und Mineralogie* **89**, 195–220.

Buerger, M. J. (1945). The genesis of twin crystals. *American Mineralogist* **30**, 469–482.

Bureau, H., Métrich, N., Pineau, F. & Semet, M. P. (1998*a*). Magma–conduit interaction at Piton de la Fournaise volcano (Réunion Island): A melt and fluid inclusion study. *Journal of Volcanology and Geothermal Research* **84**, 39–60.

Bureau, H., Pineau, F., Métrich, N., Semet, M. P. & Javoy, M. (1998*b*). A melt and fluid inclusion study of the gas phase at Piton de la Fournaise volcano (Réunion Island). *Chemical Geology* **147**, 115–130.

Bureau, H., Métrich, N., Semet, M. P. & Staudacher, T. (1999). Fluid–magma decoupling in a hot-spot volcano. *Geophysical Research Letters* **26**, 3501–3504.

Burri, C. (1935). Notiz über Zwillinge und Drillinge Gesteinbildenden Olivine. *Schweizerische Mineralogische und Petrographische Mitteilungen* **15**, 160–167.

Burton, W. K., Cabrera, N. & Frank, N. C. (1951). The growth of crystals and equilibrium structure of their surfaces. *Philosophical Transactions of the Royal Society of London, Series A* **243**, 299–358.

Cabane, H., Laporte, D. & Provost, A. (2005). An experimental study of Ostwald ripening of olivine and plagioclase in silicate melts: implications for the growth and size of crystals in magmas. *Contributions to Mineralogy and Petrology* **150**, 37–53.

Cabrera, N. & Vermilyea, D. A. (1958). The growth of crystals from solution. In: Doremus, R. H., Roberts, B. W. & Turnbull, D. (eds) *Growth and Perfection of Crystals*. Wiley, New York, pp. 393.

Chakraborty, S. (1997). Rates and mechanisms of Fe–Mg interdiffusion in olivine at 980–1300°C. *Journal of Geophysical Research* **102**, 12317–12331.

Chalmers, B. (1964). *Principles of Solidification*. New York: John Wiley.

Chernov, A. A. (1974). Stability of faceted shapes. *Journal of Crystal Growth* **24–25**, 11–31.

Clague, D. A. & Denlinger, R. P. (1994). Role of olivine cumulates in destabilizing the flanks of Hawaiian volcanoes. *Bulletin of Volcanology* **56**, 425–434.

Clocchiatti, R., Havette, A. & Nativel, P. (1979). Relations pétrogénétiques entre les basaltes transitionnels et les océanites du Piton de la Fournaise (île de la Réunion, Océan Indien) à partir de la composition chimique des inclusions vitreuses des olivines et des spinelles. *Bulletin de Minéralogie* **102**, 512–525.

Cody, A. M. & Cody, R. D. (1995). Dendrite formation by apparent repeated twinning of calcium oxalate dihydrate. *Journal of Crystal Growth* **151**, 369–374.

Coppola, D., Staudacher, T. & Cigolini, C. (2007). Field thermal monitoring during the August 2003 eruption at Piton de la Fournaise (La Réunion). *Journal of Geophysical Research* **112**, 1–15.

Coppola, D., Piscopo, D., Staudacher, T. & Cigolini, C. (2009). Lava discharge rate and effusive pattern at Piton de la Fournaise from MODIS data. *Journal of Volcanology and Geothermal Research* **184**, 174–192.

Deer, W. A., Howie, R. A. & Zussman, J. (1963). *The Rock Forming Minerals, Vol. 1.* New York: John Wiley.

Downloaded from http://petrology.oxfordjournals.org/ at University of Hawaii at Manoa Library on February 13, 2013

Deniel, C., Kieffer, G. & Lecointre, J. (1992). New ^{230}Th–^{238}U and ^{14}C age determinations from Piton des Neiges volcano, Réunion—a revised chronology for the differentiated series. *Journal of Volcanology and Geothermal Research* **51**, 253–267.

Deubelbeiss, Y., Kaus, B. J. P., Connolly, J. A. D. & Caricchi, L. (2011). Potential causes for the non-Newtonian rheology of crystal-bearing magmas. *Geochemistry, Geophysics, Geosystems* **12**, Q05007.

Dodd, R. T. & Calef, C. (1971). Twinning and intergrowth of olivine crystals in chondritic meteorites. *Mineralogical Magazine* **38**, 324–327.

Dohmen, R., Becker, H.-W. & Chakraborty, S. (2007). Fe–Mg diffusion in olivine I: experimental determination between 700 and 1,200°C as a function of composition, crystal orientation and oxygen fugacity. *Physics and Chemistry of Minerals* **34**, 389–407.

Donaldson, C. H. (1974). Olivine crystal types in harrisitic rocks of the Rhum pluton and Archean spinifex rocks. *Geological Society of America Bulletin* **85**, 1721–1726.

Donaldson, C. H. (1976). An experimental investigation of olivine morphology. *Contributions to Mineralogy and Petrology* **57**, 187–213.

Donaldson, C. H. (1977). Laboratory duplication of comb layering in the Rhum pluton. *Mineralogical Magazine* **41**, 323–336.

Donaldson, C. H. (1982). Origin of some of the Rhum harrisite by segregation of intercumulus liquid. *Mineralogical Magazine* **45**, 201–209.

Dowty, E. (1977). The importance of adsorption in igneous partitioning of trace elements. *Geochimica et Cosmochimica Acta* **41**, 1643–1646.

Dowty, E. (1980*a*). Computing and drawing crystal shapes. *American Mineralogist* **65**, 465–471.

Dowty, E. (1980*b*). Synneusis reconsidered. *Contributions to Mineralogy and Petrology* **74**, 75–84.

Dowty, E. (1987). *SHAPE*. Kingsport, TN: Shape Software, World Wide Web Address: http://www.shapesoftware.com.

Drever, H. I. & Johnston, R. (1957). Crystal growth of forsteritic olivine in magmas and melts. *Transactions of the Royal Society of Edinburgh* **58**, 289–315.

Famin, V., Welsch, B., Okumura, S., Bachèlery, P. & Nakashima, S. (2009). Three differentiation stages of a single magma at Piton de la Fournaise (Reunion hotspot). *Geochemistry, Geophysics, Geosystems* **10**, Q01007, doi:10.1029/2008GC002015.

Faure, F. & Schiano, P. (2004). Crystal morphologies in pillow basalts: Implications for mid-ocean ridge processes. *Earth and Planetary Science Letters* **220**, 331–344.

Faure, F. & Schiano, P. (2005). Experimental investigation of equilibration conditions during forsterite growth and melt inclusion formation. *Earth and Planetary Science Letters* **236**, 882–898.

Faure, F., Trolliard, G., Nicollet, C. & Montel, J.-M. (2003*a*). A developmental model of olivine morphology as a function of the cooling rate and the degree of undercooling. *Contributions to Mineralogy and Petrology* **145**, 251–263.

Faure, F., Trolliard, G. & Soulestin, B. (2003*b*). TEM investigation of forsterite dendrites. *American Mineralogist* **88**, 1241–1250.

Faure, F., Arndt, N. & Libourel, G. (2006). Formation of spinifex texture in komatiites: An experimental study. *Journal of Petrology* **47**, 1591–1610.

Faure, F., Schiano, P., Trolliard, G., Nicollet, C. & Soulestin, B. (2007). Textural evolution of polyhedral olivine experiencing rapid cooling rates. *Contributions to Mineralogy and Petrology* **153**, 405–416.

Fisk, M. R., Upton, B. G. J. & Ford, C. E. (1988). Geochemical and experimental study of the genesis of magmas of Réunion Island, Indian Ocean. *Journal of Geophysical Research* **93**, 4933–4950.

Fowler, A. D. & Roach, D. E. (1996). A model and simulation of branching mineral growth from cooling contacts and glasses. *Mineralogical Magazine* **60**, 595–601.

Fowler, A. D., Berger, B., Shore, M., Jones, M. I. & Ropchan, J. (2002). Supercooled rocks: Development and significance of varioles, spherulites, dendrites and spinifex in Archaean volcanic rocks, Abitibi Greenstone belt, Canada. *Precambrian Research* **115**, 311–328.

Harker, A. (1908). *The Geology of the Small Isles of Invernesshire. Memoir of the Geological Survey of the United Kingdom*, pp. 69–77.

Harrison, T. M. & Watson, E. B. (1984). The behavior of apatite during crustal anatexis: Equilibrium and kinetic considerations. *Geochimica et Cosmochimica Acta* **48**, 1467–1477.

Haughton, D. R., Roeder, P. L. & Skinner, B. J. (1974). Solubility of sulfur in mafic magmas. *Economic Geology* **69**, 451–467.

Helz, R. T. (1987). Diverse olivine types in lava of the 1959 eruption of Kilauea volcano and their bearing on eruption dynamics. *US Geological Survey Professional Papers* **1350(1)**, 691–722.

Hirano, N., Yamamoto, J., Kagi, H. & Ishii, T. (2004). Young, olivine xenocryst-bearing alkali-basalt from the oceanward slope of the Japan Trench. *Contributions to Mineralogy and Petrology* **148**, 47–54.

Hunter, R. H. (1987). Textural equilibrium in layered igneous rocks. In: Parsons, I. (ed.) *Origins of Igneous Layering*. Dordrecht: D. Reidel, pp. 473–503.

Hunter, R. H. (1996). Texture development in cumulate rocks. In: Cawthorn, R. G. (ed.) *Layered Intrusions*. Amsterdam: Elsevier, pp. 77–101.

Jambon, A., Lussiez, P. & Clocchiatti, R. (1992). Olivine growth rates in a tholeiitic basalt: An experimental study of melt inclusions in plagioclase. *Chemical Geology* **96**, 277–287.

Jaupart, C., Brandeis, G. & Allègre, C. J. (1984). Stagnant layers at the bottom of convecting magma chambers. *Nature* **308**, 535–538.

Kerr, A. C. & Arndt, N. T. (2001). A note on the IUGS reclassification of the high-Mg and picritic volcanic rocks. *Journal of Petrology* **42**, 2169–2171.

Kieffer, G., Tricot, R. & Vincent, P.-M. (1977). Une éruption inhabituelle (avril 1977) du Piton de la Fournaise (île de la Réunion): Ses enseignements volcanologiques et structuraux. *Comptes Rendus de l'Académie des Sciences* **285**, 957–960.

Kirkpatrick, R. J. (1975). Crystal growth from the melt: A review. *American Mineralogist* **60**, 798–814.

Kirkpatrick, R. J. (1981). Kinetics of crystallization of igneous rocks. In: Lasaga, A. C. & Kirkpatrick, R. J. (eds) *Kinetics of Geochemical Processes. Mineralaogical Society of America, Reviews in Mineralogy* **8**, 321–395.

Kohut, E. & Nielsen, R. L. (2004). Melt inclusion formation mechanisms and compositional effects in high-An feldspar and high-Fo olivine in anhydrous mafic silicate liquids. *Contributions to Mineralogy and Petrology* **147**, 684–704.

Kretz, R. (1983). Symbols for rock-forming minerals. *American Mineralogist* **68**, 277–279.

Lacroix, A. (1923). *Minéralogie de Madagascar*. Paris: Challamel.

Lacroix, A. (1936). *Le volcan actif de l'île de la Réunion et ses produits*. Paris: Gauthiers-Villars.

Land, T. A., Martin, T. L., Potapenko, S., Palmore, G. T. & De Yoreo, J. J. (1999). Recovery of surfaces from impurity poisoning during crystal growth. *Nature* **399**, 442–445.

Larsen, L. M. & Pedersen, A. K. (2000). Processes in high-Mg, high-*T* magmas: Evidence from olivine, chromite and glass in Palaeogene picrites from West Greenland. *Journal of Petrology* **41**, 1071–1098.

Le Bas, M. J. (2000). IUGS reclassification of the high-Mg and picritic volcanic rocks. *Journal of Petrology* **41**, 1467–1470.

Lénat, J.-F., Bachèlery, P. & Merle, O. (2012). Anatomy of Piton de la Fournaise volcano (La Réunion, Indian Ocean). *Bulletin of Volcanology* **74**, 1945–1961.

Liang, Y., Richter, F. M. & Watson, E. B. (1996). Diffusion in silicate melts: II. Multicomponent diffusion in CaO–Al2O3–SiO2 at 1500°C and 1 GPa. *Geochimica et Cosmochimica Acta* **60**, 5021–5035.

Downloaded from http://petrology.oxfordjournals.org/ at University of Hawaii at Manoa Library on February 13, 2013

Ludden, J. N. (1978). Magmatic evolution of the basaltic shield volcanoes of Reunion Island. *Journal of Volcanology and Geothermal Research* **4**, 171–198.

Maaløe, S. (2011). Olivine phenocryst growth in Hawaiian tholeiites: Evidence for supercooling. *Journal of Petrology* **52**, 1579–1589.

Maaløe, S. & Hansen, B. (1982). Olivine phenocrysts of Hawaiian olivine tholeiite and oceanite. *Contributions to Mineralogy and Petrology* **81**, 203–211.

Marsh, B. D. (1989). Magma chambers. *Annual Review of Earth and Planetary Sciences* **17**, 439–472.

Martin, R. F. & MacLean, W. H. (1973). Crystal growth forms in hawaiitic lavas of Heimaey, Iceland. *Geological Society of America, Annual Meeting Abstracts* **5**, 726–727.

Métrich, N., Bertagnini, A. & Di Muro, A. (2010). Conditions of magma storage, degassing and ascent at Stromboli: New insights into the volcano plumbing system with inferences on the eruptive dynamics. *Journal of Petrology* **51**, 603–626.

McDougall, I. (1971). The geochronology and evolution of the young volcanic Island of Réunion, Indian Ocean. *Geochimica et Cosmochimica Acta* **35**, 261–288.

Merle, O., Mairine, P., Michon, L., Bachèlery, P. & Smietana, M. (2010). Calderas, landslides and paleo-canyons on Piton de la Fournaise volcano (La Réunion Island, Indian Ocean). *Journal of Volcanology and Geothermal Research* **189**, 131–142.

Milman-Barris, M., Beckett, J., Baker, M., Hofmann, A., Morgan, Z., Crowley, M., Vielzeuf, D. & Stolper, E. (2008). Zoning of phosphorus in igneous olivine. *Contributions to Mineralogy and Petrology* **155**, 739–765.

Moore, J. G. & Lockwood, J. P. (1973). Origin of comb layering and orbicular structure, Sierra Nevada batholith, California. *Geological Society of America Bulletin* **84**, 1–20.

Morse, S. A. (1988). Motion of crystals, solute, and heat in layered intrusions. *Canadian Mineralogist* **26**, 209–224.

Natland, J. H. (2003). Capture of helium and other volatiles during the growth of olivine phenocrysts in picritic basalts from the Juan Fernandez Islands. *Journal of Petrology* **44**, 421–456.

Ninomiya, A. & Arai, S. (1998). Polygenetic olivine phenocrysts in Okete basanite, New Zealand. *Journal of Mineralogy, Petrology and Economic Geology* **93**, 235–249.

O'Driscoll, B., Donaldson, C. H., Troll, V. R., Jerram, D. A. & Emeleus, C. H. (2007). An origin for harrisitic and granular olivine in the Rum layered suite, NW Scotland: a crystal size distribution study. *Journal of Petrology* **48**, 253–270.

Ohnenstetter, D., Ohnenstetter, M. & Rocci, G. (1975). Tholeiitic cumulates in a high pressure metamorphic belt. *Pétrologie* **1**, 291–317.

O'Neill, H. S. C. & Mavrogenes, J. A. (2002). The sulfide capacity and the sulfur content at sulfide saturation of silicate melts at 1400°C and 1 bar. *Journal of Petrology* **43**, 1049–1087.

Passchier, C. W. & Trouw, R. A. J. (1998). *Microtectonics*. Berlin: Springer.

Peltier, A., Famin, V., Bachèlery, P., Cayol, V., Fukushima, Y. & Staudacher, T. (2008). Cyclic magma storages and transfers at Piton de la Fournaise volcano (La Réunion hotspot) inferred from deformation and geochemical data. *Earth and Planetary Science Letters* **270**, 180–188.

Peltier, A., Bachèlery, P. & Staudacher, T. (2009). Magma transport and storage at Piton de La Fournaise (La Réunion) between 1972 and 2007: A review of geophysical and geochemical data. *Journal of Volcanology and Geothermal Research* **184**, 93–108.

Petersen, J. S. (1978). Southern part of the Oslo-Rift. In: Dons, J. A. & Larsen, B. T. (eds) *The Oslo Paleorift. Norges Geologiske Undersøkelse* **337**, 171–182.

Petersen, J. S. (1985). Columnar–dendritic feldspars in the Lardalite Intrusion, Oslo Region, Norway: 1. Implications for unilateral solidification of a stagnant boundary layer. *Journal of Petrology* **26**, 223–252.

Poirier, J.-P. (1975). On the slip systems of olivine. *Journal of Geophysical Research* **80**, 4059–4061.

Pyke, D. R., Naldrett, A. J. & Eckstrand, O. R. (1973). Archean ultramafic flows in Munro Township, Ontario. *Geological Society of America Bulletin* **84**, 955–978.

Roedder, E. (1979). Origin and significance of magmatic inclusions. *Bulletin de Minéralogie* **102**, 487–510.

Roeder, P. L. & Emslie, R. F. (1970). Olivine–liquid equilibrium. *Contributions to Mineralogy and Petrology* **29**, 275–289.

Roeder, P. L., Poustovetov, A. & Oskarsson, N. (2001). Growth forms and composition of chromian spinel in MORB magma: Diffusion-controlled crystallization of chromian spinel. *Canadian Mineralogist* **39**, 397–416.

Roeder, P. L., Thornber, C., Poustovetov, A. & Grant, A. (2003). Morphology and composition of spinel in Pu'u 'O'o lava (1996–1998), Kilauea volcano, Hawaii. *Journal of Volcanology and Geothermal Research* **123**, 245–265.

Roeder, P. L., Gofton, E. & Thornber, C. (2006). Cotectic proportions of olivine and spinel in olivine-tholeiitic basalt and evaluation of pre-eruptive processes. *Journal of Petrology* **47**, 883–900.

Rohrbach, A., Schuth, S., Ballhaus, C., Münker, C., Matveev, S. & Qopoto, C. (2005). Petrological constraints on the origin of arc picrites, New Georgia Group, Solomon Islands. *Contributions to Mineralogy and Petrology* **149**, 685–698.

Romé de l'Isle, J.-B. (1783). *Cristallographie, ou description de formes propres à tous les corps du règne minéral*. Paris: Imprimerie de Monsieur.

Salaün, A., Villemant, B., Semet, M. P. & Staudacher, T. (2010). Cannibalism of olivine-rich cumulate xenoliths during the 1998 eruption of Piton de la Fournaise (La Réunion hotspot): Implications for the generation of magma diversity. *Journal of Volcanology and Geothermal Research* **198**, 187–204.

Sangwal, K. (1996). Effects of impurities on crystal growth processes. *Progress in Crystal Growth and Characterization of Materials* **32**, 3–43.

Saratovkin, D. D. (1959). *Dendritic Crystallization*. New York: Plenum.

Schiano, P. (2003). Primitive mantle magmas recorded as silicate melt inclusions in igneous minerals. *Earth-Science Reviews* **63**, 121–144.

Schwindinger, K. R. (1999). Particle dynamics and aggregation of crystals in a magma chamber with application to Kilauea Iki olivines. *Journal of Volcanology and Geothermal Research* **88**, 209–238.

Schwindinger, K. R. & Anderson, A. T. (1989). Synneusis of Kilauea Iki olivines. *Contributions to Mineralogy and Petrology* **103**, 187–198.

Servadio, Z., Villeneuve, N., Urai, M., Staudacher, T. & Gladys, A. (2008). Preliminary results of lava flow mapping using remote sensing in Piton de la Fournaise, La Réunion island. In: *Use of Remote Sensing Techniques for Monitoring Volcanoes and Seismogenic Areas, 2008. USEReST 2008,* pp. 1–4.

Shore, M. & Fowler, A. D. (1999). The origin of spinifex texture in komatiites. *Nature* **397**, 691–694.

Steno, N. (1669). *De Solido Intra Sodium Naturaliter Contento Dissertations Prodomus*, Florence. English translation by J. G. Winter *The Prodomus of Nicolaus Steno's Dissertation Concerning a Solid Body Enclosed by Process of Nature Within a Solid*. New York: Hafner, 1968.

Sunagawa, I. (1981). Characteristics of crystal growth in nature as seen from the morphology of mineral crystals. *Bulletin de Minéralogie* **104**, 81–87.

Sunagawa, I. (2005). *Crystals: Growth, Morphology and Perfection*. Cambridge: Cambridge University Press.

Downloaded from http://petrology.oxfordjournals.org/ at University of Hawaii at Manoa Library on February 13, 2013

Taubeneck, W. H. & Poldervaart, A. (1960). Geology of the Elkhorn Mountains, Northeastern Oregon: Part 2. Willow Lake intrusion. *Geological Society of America Bulletin* **71**, 1295–1322.

Thériault, R. D. & Fowler, A. D. (1995). Harrisitic textures in the Centre Hill complex, Munro Township, Ontario: Product of diffusion limited growth. *Mineralogy and Petrology* **54**, 35–44.

Toplis, M. J. (2005). The thermodynamics of iron and magnesium partitioning between olivine and liquid: Criteria for assessing and predicting equilibrium in natural and experimental systems. *Contributions to Mineralogy and Petrology* **149**, 22–39.

Upton, B. G. J., Semet, M. P. & Joron, J. L. (2000). Cumulate clasts in the Bellecombe Ash Member, Piton de la Fournaise, Réunion Island, and their bearing on cumulative processes in the petrogenesis of the Reunion lavas. *Journal of Volcanology and Geothermal Research* **104**, 297–318.

Vance, J. A. (1969). On synneusis. *Contributions to Mineralogy and Petrology* **24**, 7–29.

Viljoen, M. J. & Viljoen, R. P. (1969). The geology and geochemistry of the lower ultramafic unit of the Onverwacht Group and a proposed new class of igneous rocks. *Geological Society of South Africa, Special Publication*, Upper Mantle Project **2**, 55–86.

Villemant, B., Salaün, A. & Staudacher, T. (2009). Evidence for a homogeneous primary magma at Piton de la Fournaise (La Réunion): A geochemical study of matrix glass, melt inclusions and Pélé's hairs of the 1998–2008 eruptive activity. *Journal of Volcanology and Geothermal Research* **184**, 79–92.

Villeneuve, N., Neuville, D. R., Boivin, P., Bachèlery, P. & Richet, P. (2008). Magma crystallization and viscosity: A study of molten basalts from the Piton de la Fournaise volcano (La Réunion island). *Chemical Geology* **256**, 242–251.

Vinet, N. & Higgins, M. D. (2010). Magma solidification processes beneath Kilauea Volcano, Hawaii: A quantitative textural and geochemical study of the 1969–1974 Mauna Ulu lavas. *Journal of Petrology* **51**, 1297–1332.

Vinet, N., Flemming, R. L. & Higgins, M. D. (2011). Crystal structure, mosaicity, and strain analysis of Hawaiian olivines using *in situ* X-ray diffraction. *American Mineralogist* **96**, 486–497.

Vlastélic, I., Staudacher, T. & Semet, M. (2005). Rapid change of lava composition from 1998 to 2002 at Piton de la Fournaise (Réunion) inferred from Pb isotopes and trace elements: Evidence for variable crustal contamination. *Journal of Petrology* **46**, 79–107.

Vlastélic, I., Peltier, A. & Staudacher, T. (2007). Short-term (1998–2006) fluctuations of Pb isotopes at Piton de la Fournaise volcano (Réunion Island): Origins and constraints on the size and shape of the magma reservoir. *Chemical Geology* **244**, 202–220.

Vogt, J. H. L. (1921). The physical chemistry of the crystallization and magmatic differentiation of igneous rocks. *Journal of Geology* **28**, 318–350.

Wadsworth, W. J. (1961). The layered ultrabasic rocks of South-West Rhum, Inner Hebrides. *Philosophical Transactions of the Royal Society, London, Series B* **244**, 21–64.

Wager, L. R. & Brown, G. M. (1951). A note on rhythmic layering in the ultrabasic rocks of Rhum [Inner Hebrides, Scotland]. *Geological Magazine* **88**, 166–168.

Wager, L. R. & Brown, G. M. (1968). *Layered Igneous Rocks*. Edinburgh: Oliver & Boyd.

Wager, L. R., Brown, G. M. & Wadsworth, W. J. (1960). Types of igneous cumulates. *Journal of Petrology* **1**, 73–85.

Welsch, B., Faure, F., Bachèlery, P. & Famin, V. (2009). Microcrysts record transient convection at Piton de la Fournaise volcano (La Reunion hotspot). *Journal of Petrology* **50**, 2287–2305.

Wilkinson, J. F. G., Duggan, M. B., Herbert, H. K. & Kalocsai, G. I. Z. (1975). The Salt Lick Creek layered intrusion, East Kimberley region, Western Australia. *Contributions to Mineralogy and Petrology* **50**, 1–23.

Downloaded from http://petrology.oxfordjournals.org/ at University of Hawaii at Manoa Library on February 13, 2013